 doi:10.20944/preprints201809.0153.v1

Mesenchymal stem cell-derived exosomes ameliorated diabetic nephropathy by autophagy induction through mTOR signaling pathway

Nesrine Ebrahim[1,2], Inas A. Ahmed[3, 4], Noha I. Hussien[5], Arigue A. Dessouky[6], Ayman Samir Farid[7,*], Amal M. Elshazly[8], Ola Mostafa[1], Walaa Bayoumie El Gazzar[3], Safwa M. Sorour[9], Yasmin Seleem[9], Ahmed M. Hussein[10], Dina Sabry[11, 12]

[1]Department of Histology and Cell Biology, [2]Stem Cell Unit, [3]Department of Medical Biochemistry, [4]Molecular Biology and Biotechnology Unit, [5]Department of physiology, Faculty of Medicine, Benha University, Benha, 13518, Qalyubia, Egypt.

[6]Department of Histology and Cell Biology, Faculty of Medicine, Zgazig University, Zagazig 44519, Egypt.

[7]Department of Clinical Pathology, Faculty of Veterinary Medicine, Benha University, Moshtohor, Toukh 13736, Qalyubia, Egypt

[8]Department of Anatomy, [9]Department of Clinical Pharmacology, [10]Department of Internal Medicine, Faculty of Medicine, Benha University, Benha, 13518, Qalyubia, Egypt.

[11]Department of Medical Biochemistry, [12]Molecular Biology and Stem Cell Unit, Faculty of Medicine, Cairo University, Cairo, 11562, Egypt

E. Mails: Nesrine Ebrahim: nesrien.salem@fmed.bu.edu.eg; Inas A. Ahmed: dr.inasahmed@fmed.bu.edu.eg; Noha I. Hussien: drnohaibrahim79@gmail.com; Arigue A. Dessouky: arigueamir@yahoo.com; Ayman Samir Farid: ayman.samir@fvtm.bu.edu.eg; Amal M. Elshazly: Amal.elshazly79@yahoo.com; Ola Mostafa: ola.mostafa.moez@gmail.com; Walaa Bayoumie El Gazzar: bioch_2004@yahoo.com; Safwa M. Sorour: safwa.sorour@fmed.bu.edu.eg;

 doi:10.20944/preprints201809.0153.v1

Yasmin Seleem: yasmeen.seleem@fmed.bu.edu.eg; Ahmed M. Hussein: drdabour@yahoo.com; Dina Sabry: dinasabry@kasralainy.edu.eg

* To whom correspondence should be addressed E-mail: ayman.samir@fvtm.bu.edu.eg

Affiliation: Department of Clinical Pathology, Faculty of Veterinary Medicine, Benha University, Moshtohor, Toukh 13736, Qalyubia, Egypt

 doi:10.20944/preprints201809.0153.v1

ABSTRACT:

Background: diabetic nephropathy (DN) is a serious complication of diabetes mellitus and a common cause for end stage renal disease. Autophagy has a defensive role against kidney damage caused by hyperglycemia. The mesenchymal stem cells (MSCs) derived exosomes are currently considered as a new promising therapy in chronic renal injury. However, the renal protective mechanism of exosomes on DN has not been completely understood. We examined the potential role of MSCs derived exosomes in enhancement of autophagy activity and its effect on DN. In our study we used five groups of rats; control, DN, DN treated with exosomes, DN treated with 3-methyladenine (3-MA) and chloroquine (inhibitors of autophagy) and DN treated with 3-methyladenine (3-MA) and chloroquine and exosomes groups. We assessed renal functions, morphology and fibrosis. Moreover, autophagy markers; mTOR, Beclin-1, light chain-3 (LC3-II), and LC3-II/LC3-I ratio were detected. Additionally, electron microscopy was used for detection of autophagosomes.

Results: Exosomes markedly improved the renal functions and showed histological restoration of renal tissues with significant increase in LC3 and Beclin-1 besides the significant decrease in mTOR and fibrotic markers expression in renal tissue. All previous effects were partially abolished by the autophagy inhibitor, chloroquine and 3-MA.

Conclusions: we conclude that autophagy induction by exosomes could attenuate DN in a rat model of streptozotocin-induced diabetes mellitus.

Keywords: Diabetic nephropathy, exosomes, autophagy, mTOR

 doi:10.20944/preprints201809.0153.v1

Background:

Diabetic nephropathy (DN) is a devastating complication of diabetes mellitus and is a leading cause of end-stage renal disease (ESRD) worldwide [1]. According to statistics, nearly 347 million people have diabetes, and this number is expected to increase to 430 million by 2030 in the world. DN is becoming more and more prevalent, to some extent reaching epidemic proportions [1, 2]. Various functional and structural changes are involved in the pathogenesis of DN, including hemodynamic changes, oxidative stress, mesangial cell expansion, glomerulosclerosis, and the development of fibrosis [3]. However, despite conventional therapies, such as ameliorating hyperglycemia and hypertension, effective therapeutic strategies to counteract and reverse the progression of DN is lacking [4-6].

Current therapeutic modalities for DN are directed at controlling the diabetes-associated metabolic and hemodynamic changes to slow disease progression, while no therapy exists to repair the imminent renal damage [7]. Nevertheless, over the past decade, mesenchymal stem cells (MSCs) have gained an increasing interest as a novel regenerative therapy against renal damage [8]. MSCs have the ability to differentiate into different lineages of mesenchymal tissue [9]. The therapeutic impact of applied MSCs largely relies on released factors, including exosomes [10]. Recently, cell-derived exosomes were demonstrated to be a unique mechanism of cell-to-cell communication [11]. Exosomes are defined as vesicles derived from the plasma membrane and discharged in the microenvironment by several cell types including stem cells and their progenitors [12]. Exosomes also transport micro-RNA (mi-RNA) and mRNA, which may induce epigenetic changes in target cells [13]. In addition, exosomes may enhance an angiogenic program in endothelial cells or regulate the phenotypes of cells injured by a horizontal transfer with mi-RNA or mRNA [14].

Preprints (www.preprints.org) | NOT PEER-REVIEWED | Posted: 10 September 2018 doi:10.20944/preprints201809.0153.v1

Macroautophagy (hereafter referred to as autophagy) is an evolutionarily conserved homeostatic process that mainly plays a role in damaged organelle degradation and intracellular content digestion [15]. Autophagy is a tightly regulated process which eliminates cytotoxic protein aggregates and damaged organelles through lysosomal degradation and allows cells to recycle mitochondrial energy sources and maintain survival [15]. Impairment of autophagy in renal cells, particularly podocytes and tubular cells, has been implicated in pathogenesis of various kidney diseases, including DN [16]. Therefore, improvement and/or restoration of autophagy are considered as promising therapeutic targets for DN [17].

There is a growing evidence that the pathogenesis of DN is associated with impaired autophagic activity via activation of the mTOR (mechanistic target of rapamycin) pathway [18]. mTOR is the classical nutrient-sensing pathway regulating autophagic activity through its association with two distinct protein complexes, mTOR complex 1 (mTORC1) and mTORC2. In general, mTORC1 is a negative regulator of autophagy by inhibiting the activity of the ULK1 complex through direct phosphorylation. Nutrient starvation induces autophagy primarily through the inhibition of mTORC1 [19]. Enhanced mTORC1 activity is seen in human and experimental type 1 and type 2 DN [20-22]. Thus, in the present study, we evaluated the effects of MSC derived exosomes in ameliorating histological alterations in DN and to clarify their role in inducing autophagy by modulating mTOR signaling pathway.

Results:

Exosomes characterization:

A transmission electron microscopic examination of purified exosomes demonstrated their characteristic spheroid double membrane bound morphology with a diameter of 40-100 nm (Fig. 2A). Also, the exosomes were detected in renal tissues by PKH26 dye tracing (Fig. 2B). The

Preprints (www.preprints.org) | NOT PEER-REVIEWED | Posted: 10 September 2018 doi:10.20944/preprints201809.0153.v1

amount of purified exosome was significantly (*P<0.05*) increased over the passages and reach maximum concentration in the third passage which used for administration to rats (Fig. 2C and D).

Biochemical analysis:

Examination of all subgroups of the control group showed similar results regarding biochemical examinations; therefore, results of subgroup Ia were used to represent this group. Injection of STZ resulted in a significant increase in blood glucose, serum creatinine, blood urea nitrogen (BUN) and urinary albumin excretion at the end of the 6^{th}, 8^{th}, 10^{th} and 12^{th} weeks compared to control group ($P<0.05$) (Fig. 3). Injection of exosomes caused a significant decrease ($P<0.05$) in blood glucose, serum creatinine, BUN and urinary albumin excretion at the 10^{th} and 12^{th} week compared with the DN group. On the other hand, treatment of DN with 3-MA and chloroquine aggravated the effects of injected STZ and reduce the protective effects of exosome indicated by a significant ($P<0.05$) increase in blood glucose, serum creatinine, BUN and urinary albumin excretion at 10^{th} and 12^{th} weeks when compared with the DN and exosome-treated groups. On the same context, DN group treated with 3-MA and chloroquine and exosome showed significant ($P<0.05$) increases in blood glucose, serum creatinine, BUN and urinary albumin excretion at 10^{th} and 12^{th} weeks when compared with the exosome-treated group.

Histological examination:

Light microscope examination:

H&E:

Sections of ***group I*** (Control group) revealed renal corpuscles consisting of glomeruli surrounded by narrow Bowman's space and Bowman's capsule. The corpuscles were surrounded by proximal and distal convoluted tubules (Fig. 4A). ***Group IIa*** (DN group at the end of 8^{th} week):

Preprints (www.preprints.org) | NOT PEER-REVIEWED | Posted: 10 September 2018 doi:10.20944/preprints201809.0153.v1

The renal tissues showed numerous glomeruli with mesangial expansion and glomerular nodular sclerosis (Kimmelstien Wilson nodules) which appeared as acidophilic nodules with palisading nuclei at their periphery of glomeruli. Many tubules demonstrated darkly stained nuclei (Fig. 4B). Also, sections of ***Group IIb*** (DN group at the end of 12th week) demonstrated shrunken glomeruli with wide Bowman's spaces (glomerulosclerosis). The tubules showed swollen epithelial lining obliterating their lumens in addition to darkly staining nuclei. Some nuclei were basal while the others where apical (Fig. 4C). The renal corpuscles of ***Group III*** *(DN+3-MA&Chloroquine)* showed marked shrinkage of glomeruli with obvious widening of the Bowman's spaces (glomerulosclerosis). The tubules showed swollen tubular epithelium obliterating the lumen and darkly stained nuclei with loss of their polarity (some nuclei were basal while the others where apical) (Fig. 4D). Glomeruli of ***Group IV*** (*DN+exosomes*) exhibited a decreased mesangial expansion. The tubules showed open lumens and normal nuclear polarity (basal nuclei) of their lining epithelium (Fig. 4E). ***Group V*** (*DN+3-MA&Chloroquine+exosomes*) demonstrated persistent mesangial expansion with swollen tubular epithelial lining, obliterated lumens and darkly staining nuclei with loss of nuclear polarity (Fig. 4F).

Masson's trichrome stain:

Masson's trichrome stained sections of ***group I*** (Control group) demonstrated minimal amounts of collagen fibers among the glomerular capillaries and surrounding the renal corpuscles and tubules (Fig. 5A). ***Group IIa and IIb*** (DN groups) and ***Group III*** (*DN+3MA&Chloroquine*) showed an obvious increase in the amount of collagen fiber deposition among the glomerular capillaries and between the tubules with a greater increase observed in ***Group III*** (Fig. 5B, C &D). On the other hand, ***Group IV*** (*DN+exosomes*) revealed decreased amounts of collagen fibers

Preprints (www.preprints.org) | NOT PEER-REVIEWED | Posted: 10 September 2018 doi:10.20944/preprints201809.0153.v1

among the glomerular capillaries and surrounding the renal corpuscles and tubules (Fig. 5E), while ***Group V*** (*DN+3MA&Chloroquine+exosomes*) demonstrated persistent increase in collagen fibers among the glomerular capillaries and surrounding the renal corpuscles and tubules (Fig. 5F).

Immunohistochemical study:

The immunohistochemical reaction for TGF-β in ***Group I*** showed a minimal positive cytoplasmic reaction in the tubular epithelial cells (Fig. 6A). In ***Group IIa***, the tubular cells showed a moderate positive cytoplasmic reaction (Fig. 6B), while the reaction was strong positive in tubular cells of ***Group IIb*** (Fig. 6C). Tubular epithelial cells of ***Group III*** showed an intense positive cytoplasmic reaction (Fig. 6D). On the other hand, ***group IV*** revealed a mild positive cytoplasmic reaction (Fig. 6E), while ***Group V*** showed a moderate positive cytoplasmic reaction (Fig. 6F).

Morphometric analysis:

The mean area percent of collagen fiber deposition and TGF-β immuno-expression for all groups is presented in Fig. 6G & 4G. Diabetic nephropathy group (**Group IIa & IIb**) and group III showed a significant increase in the mean area percentage of collagen fibers deposition and TGF-β immuno-expression compared to control group. Furthermore, administration of exosomes caused a significant decrease in the mean area percent of collagen fibers deposition and TGF-β immuno-expression compared to both DN groups (**group IIa & IIb**). On the contrary, administration of 3-MA and chloroquine caused a significant decrease in the anti-fibrotic effects of exosomes as evidenced by a significant increase in the mean area percent of collagen fibers deposition and TGF-β immuno-expression compared to exosomes treated group.

Preprints (www.preprints.org) | NOT PEER-REVIEWED | Posted: 10 September 2018 doi:10.20944/preprints201809.0153.v1

Transmission electron microscopic study:

The ultrastructure of glomerular filtration barriers of ***Group I*** (Control group) consisted of thin fenestrated endothelial cells, thin regular glomerular basement membranes in addition to the foot processes of the podocytes (Fig. 7A). ***Group IIa and IIb*** (DN groups) demonstrated extensive fusion and effacement of the foot processes in addition to diffuse thickening of the glomerular basement membrane (Fig. 7B & C). ***Group III*** (*DN+3-MA&Chloroquine*) showed that glomerular basement membranes had extensive areas of irregular thickening with area of thickening, fusion and effacement of the foot processes (Fig. 7D). ***Group IV*** (*DN+exosomes*) revealed thin regular glomerular basement membranes in addition to the foot processes of the podocytes (Fig. 7E). On the other hand, ***Group V*** (DN+3-MA&Chloroquine+exosomes) revealed persistent thickening of the glomerular basement membranes and fusion and effacement of podocytes in many areas (Fig. 7F).

The proximal tubular epithelial cells of ***Group I*** (Control group) were seen resting on thin regular basement membranes. They possessed numerous tightly packed apical microvilli, round euchromatic nuclei and numerous mitochondria in the cytoplasm (Fig. 8A). Tubular cells of ***Group IIa*** (DN group after 8 weeks) rested on slightly thickened basement membranes. Their apical microvilli appeared swollen and disrupted and the nuclei were shrunken. The cytoplasm contained areas of rarefaction in addition to numerous swollen mitochondria and scattered dense bodies (Fig. 8B). ***Group IIb*** (DN group after 12 weeks) revealed increased thickening of the tubular basement membranes with disrupted apical microvilli and pyknotic nuclei. The cytoplasm contained multiple variable sized vacuoles, variably sized mitochondria and few scattered electron dens bodies (Fig. 8C). ***Group III*** (DN+3-MA&Chloroquine) showed tubular epithelial cells resting on

Preprints (www.preprints.org) | NOT PEER-REVIEWED | Posted: 10 September 2018 doi:10.20944/preprints201809.0153.v1

a thickened basement membrane with swollen and disrupted apical microvilli. The cytoplasm contained numerous swollen mitochondria of various sizes and shape with few electron dense bodies. The nuclei contained peripheral clumps of heterochromatin. Also, the interstitium revealed abundant collagen fibrils (Fig. 8D). ***Group IV*** (*DN+exosomes*) showed the tubular cells resting on thin basement membranes. The apical microvilli were numerous and tightly packed, and the nuclei appeared round and euchromatic. The cytoplasm contained numerous autophagosomes containing cellular debris, numerously scattered electron dense bodies and elongated mitochondria (Fig.6E). While ***Group IV*** (*DN+3MA&chloroquine+exosomes*) tubular cells showed persistent thickening of the tubular basement membranes in many areas, swollen apical microvilli and slightly shrunken nuclei. The cytoplasm showed areas of rarefication in addition to variably sized mitochondria and scattered electron dense bodies (Fig.8F).

Gene expression results of LC3II, mTOR and Beclin 1 genes in all experimental groups:

Gene expression of LC3II, mTOR and Beclin 1 genes presented in figure 9. DN group showed significant (P<0.05) down-regulations of LC3 and Beclin 1 with a significant (P<0.05) upregulation in mTOR gene expression in renal tissues compared to control group. Furthermore, treatment of DN with exosomes caused significant (P<0.05) upregulations in Beclin 1 and LC3 as well as significant (P<0.05) down-regulations in mTOR gene expression in renal tissues when compared with DN group. On the other hand, injection of both 3-MA and chloroquine caused significant (P<0.05) down-regulations in autophagy markers, Beclin-1 and LC3 with a significant (P<0.05) upregulation in mTOR mRNA in renal tissues compared to exosomes-treated group.

mTOR, LC3-I, LC3-II, fibronectin, TGF-β and β-actin detection by Western blotting:

Preprints (www.preprints.org) | NOT PEER-REVIEWED | Posted: 10 September 2018 doi:10.20944/preprints201809.0153.v1

As shown in figure 10, protein expressions of mTOR, fibronectin and TGF-β in the DN group were significantly (P<0.05) higher than in control group, and exosomes treatment significantly (P<0.05) reduced their levels. On the other hand, the ratio of LC3-II and LC3-I protein expression (Fig. 10.B) in the DN group decreased significantly when compared with the control group, while exosomes treatment significantly enhanced LC3-II/LC3-I protein expression compared to the DN group (P<0.05). Furthermore, injection of both 3-MA and chloroquine resulted in a significant increase in fibronectin, TGF-β and mTOR protein expression and a significant decrease LC3-II protein expression compared with the exosomes-treated group.

Discussion:

The rapidly increasing prevalence of diabetes is resulting in a concomitant increase in the prevalence of DN [23]. Given the large worldwide health care burden associated with DN, there has been much interest in the search for novel treatment targets. Therefore, in latest decades, many researches have been making a lot of efforts to recognize the molecular mechanisms elaborated in initiation and progression of diabetic nephropathy to develop novel therapeutic approaches. However, the end-stage kidney disease due to DN remains to increase worldwide. There are urgent needs to find additional novel therapeutic goals for prevention of DN [24, 25]; hence, the present study for the first time demonstrated that MSCs derived exosomes could ameliorate DN by autophagy regulation through the mTOR signaling pathway *in vivo* in kidneys of diabetic rat.

The current study showed marked deteriorations in renal functions in DN rats indicated by significant increases in serum creatinine, BUN and urinary albumin excretion (Fig. 3) supported with the histological lesions of classical DN which were demonstrated by light (Fig. 4, 5 and 6)

 doi:10.20944/preprints201809.0153.v1

and electron microscopy (Fig. 7 and 8) in the form of thickening of the glomerular basement membrane and mesangial expansion, deformity of filtration barrier and interstitial fibrosis with diffuse glomerular sclerosis. These findings coincide with the previous reports from patients with DN [26, 27]. Glomerular cell loss is considered to be a result of diabetes-induced nephrotoxicity [28]. Furthermore, diabetes-induced nephrotoxicity affects the blood vessel diameter, a vasodilatation effect [29]. Glomerular vasodilatation could induce a podocyte mechanical stretch leading to foot process effacement and, after that, cellular detachment. In agreement to what has been published before [30, 31], podocyte stretch induces a decreased podocyte nephrin expression, the main slit diaphragm protein, leading to disturbances in the glomerular filtration function and proteinuria. Furthermore, accumulation of edematous fluids in diabetic patients induces an increase in Bowman's space. The two main causes of glomerular edema formation are the increased movement of renal fluid from the glomerular pool to the urinary pool and blockade of the renal tubular system. As described before [32, 33], dilated glomerular vessels could increase the vascular endothelium fenestrae leading to increased fluid movements from the glomerular pool to the urinary pool inducing edema formation. Additionally, Lenoir et al., 2015 [34] showed mesangial expansion and glomerulosclerosis by histological analysis and glomerular basement membrane thickening, podocyte foot process broadening and effacement by TEM in endothelial cell-specific Atg5-deficient diabetic glomeruli.

Autophagy that generated by various harmful factors contributes to maintenance of cell homeostasis. Autophagy principally serves an adaptive, or a ‘programmed cell survival' mechanism to protect organisms during periods of enhanced cellular distress [35]. In our study, the deterioration of renal functions, in DN group, possibly caused by defect(s) in the autophagy process. We evaluated LC3, beclin-1 and mTOR as well as TEM examination of autophagosomes

 doi:10.20944/preprints201809.0153.v1

as proper procedures for monitoring autophagy [36]. The present study demonstrated significant downregulations of autophagy markers, LC3 and beclin-1, in renal tissue, as well as a significant upregulation of mTOR expression in the DN rats compared with the controls (Fig. 9). These outcomes are in concurrence with those of Fang et al. [37] who found that the renal expression of autophagy related proteins including beclin-1, and LC3 were markedly suppressed in rats with DN. Also, the findings of present study support the findings of Gödel et al. 2011 [38] who reported significant upregulations of mTOR itself and mTORC1- target genes, in human patients with progressive DN, as compared to the controls. Gödel and his colleagues also demonstrated that activation of mTORC1 inhibits diabetes-related autophagy in renal tissues of diabetic mice and patients. Nowadays, the gold standard for autophagy monitoring is the TEM, the only technique able to elucidate the real presence of subcellular autophagic structures like autophagosome, lysosome, and autophagolysosome [36, 39]. In the current study, TEM showed rare autophagic vacuoles in the tubular cells of DN group compared to the control group (Fig. 7 and 8). In line with these results, Lenoir et al., 2015 [34] who evaluated the role of autophagy in the endothelial cells of diabetic kidneys using endothelial cell-specific Atg5-deficient mice. Lenoir explained that the ultrastructural analysis exhibited glomerular endothelial cell cytoplasmic disorganization and vacuolization as well as detached cells, most likely endothelial cells, in the lumen of the capillaries in the glomeruli of endothelial cell-specific Atg5-deficient diabetic mice.

As a central element signaling cell growth and enhancing protein translation, the mammalian target of rapamycin (mTOR), when inhibited, induces autophagy. Likewise, as a critical feedback mechanism, reactivation of mTOR terminates autophagy and initiates lysosome reformation [35]. In our study we found that DN suffered rats showed a significant up-regulation in mTOR mRNA as well as protein expressions. This upregulation is aggravated in the presence of 3-

 doi:10.20944/preprints201809.0153.v1

MA&Chloroquine administration and alleviated in the presence of exosome treatment (Fig. 9 and 10). Numerous studies have revealed that hyperactivation of the mTOR pathway in DN shows an essential role in glomerular and tubular cells hypertrophy [40, 41] and is related with injury of podocyte and decline of glomerular filtration rates. A growing number of studies have suggested that mTORC1 pathway inhibition with rapamycin has renoprotective impacts on the DN progression in models of type 1 [42] and type 2 diabetes [43]. Overactivation of mTOR resulted from prolonged exposure to hyperglycemia, which is a crucial player in diabetic kidney injury [44, 45]. These studies demonstrated that the over-activation of mTOR in the podocytes results in albuminuria due to the widening of glomerular basement membrane, mesangial expansion, and collagen deposition. Also, they showed that the mTORC1 hyperactivity in podocytes disrupts the localization of the proteins constructing the filtration slits, with eventual increased glomerular permeability to macromolecules. Additionally, other studies attributed progressive renal tissue injury to activation of mTORC1 and so suppression of autophagy and explained this issue by different mechanisms; First, defective autophagy impairs clearance of advanced glycation end-products (AGEs) [46] and damaged mitochondria in podocytes [47]. Second, autophagic insufficiency, further increases hypoxia and endoplasmic reticulum (ER) stress, thus increases vulnerability of the tubular cells [46, 48]. Third, suppressed autophagy leads to collagen accumulation due to defective degradation [47].

More importantly, the suppression of autophagy, due to mTOR activation, was reported by Fang.et al. 2013 [37] who reported that autophagy initiation is triggered by the action of unc-51-like kinase (Ulk)-1 (mammalian ortholog of the yeast Atg1), which binds to and phosphorylates other autophagy essential proteins. However, exposure to hyperglycemia, leads to activation of mTORC1, which in turn phosphorylates and inactivates the Ulk-1, thus prevents initiation of

 doi:10.20944/preprints201809.0153.v1

autophagosome formation [49]. Of note, mTORC1 activation does not only inhibit autophagy, but also is implicated in synthesis of proteins and other macromolecules. It has been reported that activated mTOR enhances interstitial fibrosis in diabetic kidneys [20]. These findings go parallel to that of the present study, as we demonstrated a significant increase in TGF-β1 and fibronectin protein expression (Fig. 10) and collagen fibers deposition among the glomerular capillaries and surrounding the renal corpuscles and tubules, in renal specimens stained by Masson's Trichrome stain in DN rats as compared to control ones (Fig. 5). It has been suggested that hyperglycemia-activated mTORC1, stimulates the fibroblasts proliferation and collagen synthesis. Furthermore, it enhances the expression of profibrotic cytokines, such as TGF-β1 and connective tissue growth factor, resulting in progressive fibrosis and tubulointerstitial changes in DN [20]. Fibrosis considered as a major source of the pathogenesis of DN. Myofibroblasts play a vital role in fibrosis induction of the glomerulus and renal tubulointerstitium. Epithelial-to-mesenchymal transition (EMT) is a main source of the myofibroblasts in podocytes and proximal tubular cells in DN. TGF-β is a key regulator not only of EMT induction but also the synthesis of extracellular matrix molecules such as fibronectin, collagen type I, and laminin, causing renal fibrosis. Therefore, regulation of TGF-β is a potential therapeutic target for DN [50].

The results of the present study also demonstrated that multiple injections of exosomes, in group IV, significantly improved the renal functions of DN group indicated by significant decreases in serum creatinine, BUN and urinary albumin (Fig. 3). Moreover, renal histological changes improved in the form of decreased mesangial expansion and open-walled tubules (Fig. 4) with a significant decrease in collagen expression by Masson's Trichrome and TGF-β immunoexpression (Fig. 5). These results were supported by TEM which demonstrated multiple autophagic vacuoles, euchromatic nuclei, scattered mitochondria, and closely packed apical

 doi:10.20944/preprints201809.0153.v1

microvilli in proximal tubules epithelial cells (PTEC). Also, there were nearly normal glomerular basement membrane with nearly normal podocyte and more thinning of glomerular filtration barrier (Fig. 6 and 7).

These results were in accordance to Nassar et al [51] who demonstrated that the administration of MSCs could reverse DN through paracrine mechanisms rather than by MSC transdifferentiation. MSC derived exosomes might be such a paracrine mechanism for cell-to-cell communication. Evidence from previous studies, indicates that MSCs mediate their paracrine effects via release of exosomes that deliver their cargo of various mRNAs, miRNAs and proteins to recipient cells [52]. Also, Nagaishi et al. 2016 [53] proofed the kidney that received exosome injection exhibited improvement in histological picture of DN in the form of decreased degeneration, vacuolation, atrophic changes and inflammatory cells infiltration of PTEC confirmed by H&E staining and PAS staining with decreased fibrous components confirmed by Azan staining.

The nephroprotective effect of exosomes explained by Bruno et al., 2012 [52] who revealed that the exosomes derived from MSCs demonstrate protective effects in acute renal injury via the transportation of a specific subset of cellular mRNAs, which are associated with the mesenchymal phenotype and with the control of transcription, proliferation, and immunoregulation. Also, Bruno et al. reported that exosomes activated a proliferative program of PTEC and inhibited apoptosis via inducing the synthesis of hepatocyte growth factor and macrophage-stimulating protein by the horizontal transfer of mRNAs packed in exosomes.

However, the accumulation of autophagic vacuoles did not always mean increased the autophagosomes formation and may denote inhibited autolysosomes maturation, so LC3-II detection via Western blotting were valuable in monitoring the autophagosomes number [25],

Preprints (www.preprints.org) | NOT PEER-REVIEWED | Posted: 10 September 2018 doi:10.20944/preprints201809.0153.v1

therefore, we detected the autophagosome formation-related proteins (the LC3 conversion and Beclin-1). We found that DN group showed significant decreases in the expression level of LC3 and Beclin-1 compared with control. Exosome-treated DN rats significantly increased the expression of Beclin-1 mRNA as well as the LC3-II/LC3-I protein expression ratio, indicating increased autophagosome formation (Fig. 10). Accordingly, our results revealed that injections of exosomes upregulated the expression of the autophagy markers LC3 and Beclin-1 and downregulated the mTOR, in group IV as compared to rats of DN group suggesting that exosomes may activate autophagy by decreasing the mTOR. These results run parallel to earlier study which reported that genetic reduction of mTOR levels, in mTORC1 knockout mice, significantly reduced the effects of mTOR hyperactivation in renal tissues and suppressed the progression of DN in diabetic animals [43].

In this context, our data were in accordance with earlier results of Liu and his colleagues [54] showed that MSCs-derived exosomes significantly reduced the expression of phosphorylated mTOR/ mTOR in rat cardiomyocytes after ischemia reperfusion injury. They attributed the enhanced autophagic activities in exosome treated cells, partly to inhibition of mTOR pathway. These results provide a possible explanation to the improved biochemical and histological features of DN in group IV.

Regarding the effects of exosomes on renal fibrosis induced by diabetes, repeated injection of MSC-derived exosomes in group IV caused significant decrease in the immunoexpression of TGF-β1 and collagen fibers deposition between glomeruli and tubules of renal samples stained by Masson's Trichrome stain and these findings confirmed by significant decrease in protein expression of TGF-β and fibronectin by western blot. Such results suggest that multiple injections of exosomes exhibit a potent anti-fibrotic effect, and therefore may improve renal function,

 doi:10.20944/preprints201809.0153.v1

indirectly by reducing disease associated fibrosis. These outcomes run parallel to former reports [17] suggesting that barricade of the mTOR pathway decreased TGF-β1 in the kidney. Previous study showed that exosomes with selective micro RNAs patterns, improved renal function and reversed TGF-β1-morphological changes in renal cells [53]. Thus, MSC-derived exosomes provide a new potentially effective therapeutic approach to slow down the progression of renal disease and improve renal function by modulating autophagy.

To confirm the role of autophagy in mediating the protective impact of exosomes on DN, we used both 3-MA and chloroquine, autophagy inhibitors, in groups III and V. Our study demonstrated that both 3-MA and Chloroquine (CQ) are beneficial in inhibiting the process of autophagy (group III). 3-MA is an early autophagy inhibitor, which could suppress the activity of type III of phosphoinositide-3-kinase (PI3K) inhibitors and the formation of autophagosome so as to inhibit autophagy [55]. While, chloroquine reverses autophagy by inhibiting lysosomal acidification, results in lysosome accumulation and autophagy blockade [56]. We used both 3-MA and chloroquine to be sure of autophagy inhibition because, previous study revealed that in nutrient rich conditions, such as ours, 3MA may even stimulate autophagy flux instead of blocking it [57].

Treatment of DN rats with chloroquine and 3-MA (group III) resulted in significant downregulations of LC3 and Beclin-1 (Fig. 9). In addition, there was reduction in the number of autophagic vacuoles confirmed by TEM when compared to exosomes treated group (Fig. 7 and 8), indicating that autophagy was inhibited by 3-MA and chloroquine. Furthermore, pretreatment with chloroquine and 3-MA exacerbated renal insult manifested with significant increase in serum creatinine, BUN and urinary albumin (Fig. 3) in parallel with deterioration of renal histology (Fig. 4 and 5). Such deterioration was evidenced by persistent mesangial expansion, swollen tubular epithelial lining with obliteration of their lumens and darkly staining nuclei with loss of their

 doi:10.20944/preprints201809.0153.v1

polarity. Inhibition of autophagy by chloroquine not only decreased the protective effect of exosomes on renal function (Group V), but also it decreased its antifibrotic effect indicated by significant increase in the protein expression of TGF-β (Fig. 6) and fibronectin (Fig. 10) with collagen fibers deposition (Fig. 5) leading to persistent thickening of the glomerular basement membranes in many areas when compared to exosomes treated group. In this context, our data were in accordance with earlier results of Verschooten and his colleges 2012 showed the chloroquine is an autophagy inhibitor enhancing the cell death inducing effect of the Flavonoid Luteolin in metastatic squamous cell carcinoma cells. While, combined treatment of chloroquine and 3-MA with exosomes in group V alleviated the finds found in group III [58].

Conclusions:

In conclusion, the potential nephroprotective effects of MSCs-derived exosomes in diabetic nephropathy model based on their ability to upregulate autophagy by suppression of the mTOR pathway, and by its antifibrotic effect. These findings provide a basis for the future use of exosomes as a new biological therapeutic approach for DN.

Methods

Experimental animals:

Adult male Albino rats (250-270 g), 8 weeks of age, were purchased from the Experimental Animal Unit, Faculty of Veterinary Medicine, Benha University, Egypt. The rats were bred and maintained in an air-conditioned animal house under specific pathogen-free conditions. All animals were housed in clean cages and given a standard diet and clean water *ad libitum.* The rats were subjected to a normal light/dark cycle (12-h light-dark cycle starting at 8:00 AM) and room

Preprints (www.preprints.org) | NOT PEER-REVIEWED | Posted: 10 September 2018 doi:10.20944/preprints201809.0153.v1

temperature (23 ± 3 °C) and allowed free access to chow and water. This study was carried out in strict accordance with the recommendations in the Guide for the Care and Use of Laboratory Animals of the National Institutes of Health (NIH publication No. 85– 23, revised 2011). All protocols were approved by the institutional review board for animal experiments of the Faculty of Medicine, Benha University, Egypt.

Preparation of MSCs derived exosomes:

MSCs derived exosomes were obtained from supernatants conditioning media of MSCs. Firstly, rat bone marrow derived MSCs (BM-MSCs) were prepared in the Central Lab, Faculty of Medicine, Benha University [52]. The MSCs were cultured in DMEM without FBS but with 0.5 % human serum albumin (HSA) (Sigma-Aldrich) overnight. The viability of the cell cultured overnight was more than 99 % as detected by trypan blue exclusion. Cells were plated at 4000 cells/cm2 for 7 days. On day 7, cells were trypsinized, counted, and replated in expansion medium at the density of 2000 cells/cm2 for another period of 7 days (end of passage 1). The expansion was performed until reaching third passage.

The conditioned medium was collected and stored at -80°C. The medium was centrifuged at 2,000 g for 20 min to remove debris, and then ultracentrifuged at 100,000 g in a SW41 swing rotor (Beckman Coulter, Fullerton, CA, USA) for one hour at 4°C. Exosomes were washed once with serum free M199 (Sigma-Aldrich) containing 25 mM HEPES (pH = 7.4) and submitted to a second ultracentrifugation in the same conditions. Exosomes were labeled with PKH26 fluorescent linker dye to trace them in vivo. Exosomes were stored at -80°C for the experiment.

Preprints (www.preprints.org) | NOT PEER-REVIEWED | Posted: 10 September 2018 doi:10.20944/preprints201809.0153.v1

Characterization of MSCs derived exosomes:

- **Exosomes labeling with PKH-26:**

Exosomes were isolated from the supernatant of first, second and third passages of MSCs cultured in α-MEM deprived of FBS. The MSCs derived exosomes were fixed with 2.5% glutaraldehyde in HSA for 2 h. After they were washed; exosomes were ultra-centrifuged and suspended in 100 µL HSA. A total of 20 µL of exosomes was loaded onto a formvar/carbon-coated grid, negatively stained with 3% aqueous phosphor-tungstic acid for one minute and observed by transmission electron microscopy (HITACHI, H-7650, Japan) [59]. The protein content of exosomes pellet was quantified by the Bradford method (BioRad, Hercules, CA) [59]. The dose of injected EVs was adjusted to 100 µg protein/suspended in 0.2 ml PBS [60]. Additionally, PKH26 (Sigma-Aldrich, St. Louis, MO, USA) was done to confirm the exosome localization within the renal tissue. The exosomes pellet was diluted with PKH-26 kit solution to 1 mL and 2 µL of fluorochrome were added to this suspension and incubated at 38.5°C for 15 min. After that, 7 mL of serum-free HG-DMEM were added to the suspension then it was ultracentrifuged for second time at 100,000 g for 1 h at 4°C. The final pellet was resuspended rapidly in HG-DMEM and stored at −80°C for future injection in experimental induced rat [61].

- **Western blot for characterization of exosomes:**

The antibody used was antigen affinity-purified polyclonal sheep IgG anti-rabbit CD81 (Biolegend, Cat N: 0349509). Protein isolated from isolated exosomes using RIPA buffer. Twenty ng of protein was loaded and separated by SDS-PAGE on 4-20% polyacrylamide gradient gels. Following incubation, in 5% non-fat dry milk, Tris-HCl, 0.1% Tween 20 for 1 hr, the CD81 polyclonal monoclonal antibody was added to one of the membranes including specimen samples and incubated at 4 ℃ overnight. The appropriate secondary antibody was incubated for 2 hr at room

Preprints (www.preprints.org) | NOT PEER-REVIEWED | Posted: 10 September 2018 doi:10.20944/preprints201809.0153.v1

temperature. After being washed twice n 1 x TBS-T, densitometric analysis of the immunoblots was performed to quantify the amounts of CD81 and CD63 against housekeeping protein β-actin by Image analysis software on the ChemiDoc MP imaging system (version 3) produced by Bio-Rad (Hercules, CA).

Experimental chemicals:

- ***Streptozotocin*** powder was obtained from Sigma-Aldrich Chemical Co. (St. Louis, Missouri, USA). The powder was stored at -20°C, and the amount needed was dissolved in 0.1 mol/l citrate buffer, pH 4.5 immediately before use.
- ***3-Methyladenine*** was purchased from (Sigma-Aldrich, St Louis, Missouri, USA) in powder form. The powder was dissolved in distilled water, and then placed in 50°C bath water.
- ***Chloroquine diphosphate*** salt was purchased from (Sigma-Aldrich, St Louis, Missouri, USA) in powder form. The powder was dissolved in distilled water.

Induction of DN:

Type I diabetes was induced in overnight fasted rats by a single intraperitoneal (I.P.) injection of freshly prepared STZ (60 mg/kg, dissolved in 0.1 M cold citrate buffer, pH 4.5). After STZ injection, rats acquired drinking water containing sucrose (15 g/L) for 48 hours, to lessen the early death due to insulin discharge from partially injured pancreatic islets. Seventy-two hours later, rats were checked for hyperglycemia and those with fasting blood sugar more than 250 mg/dL were included in the study. Diabetic rats received long-acting insulin (2-4 U/rat) via subcutaneous

Preprints (www.preprints.org) | NOT PEER-REVIEWED | Posted: 10 September 2018 doi:10.20944/preprints201809.0153.v1

injection to maintain blood glucose levels in a desirable range (350 mg/dL) and to avoid subsequent development of ketonuria [62].

Experimental design and treatment protocol:

The experimental design is shown in Fig.1. Fifty-six male rats were randomly divided into five groups as follows:

Group I (Control group; *n*=21): Rats were fed a regular chow diet for twelve weeks. The rats were divided equally into 3 subgroups of 7 rats each as follows:

Subgroup IA: The rats were left without intervention.

Subgroup IB: The rats were injected intraperitoneally (I.P.) with a single dose of 0.25 ml/kg body weight sodium citrate buffer (vehicle of STZ).

Subgroup IC: The rats were injected intraperitoneally (I.P.) with distilled water for 4 weeks (vehicle of Chloroquine diphosphate). Simultaneously they were intravenously (I.V.) injected with 0.2 ml phosphate buffer saline (PBS), one injection at the 8th week and the other injection at the 10th week of the experiment (vehicle of exosomes).

Group II (DN group; *n*=14): DN was induced and the rats subdivided equally into 2 subgroups:

Group IIA: DN was induced and rats were scarified at the end of the 8^{th} week of the experiment to confirm histological changes of DN.

Group IIB: DN was induced and rats were scarified at the end of experiment at the 12^{th} week.

Group III (DN+3-MA&Chloroquine; *n*=7): DN was induced and rats were intraperitoneally injected with 3-MA (10 mg/ kg) and Chloroquine (40 mg/ kg) [63] once per day for 4 weeks from the 8^{th} week till the end of the experiment.

Preprints (www.preprints.org) | NOT PEER-REVIEWED | Posted: 10 September 2018 doi:10.20944/preprints201809.0153.v1

Group IV (DN+exosomes; *n*=7): DN was induced and rats treated with two injections of exosomes (100 µg/kg/dose suspended in 0.2 ml PBS through tail vein injection) [60] the first injection was at the 8th week of the experiment and the second one at the end 10th week of experiment (12).

Group V (DN+3-MA&Chloroquine+exosomes; *n*=7): DN was induced and rats were intraperitoneally injected with 3-MA (10 mg/ kg) and Chloroquine (40 mg/ kg) once per day for 4 weeks from the 8th week till the end of the experiment. Simultaneously, the exosomes were injected at 8thand 10th weeks of experiment.

Sampling:

Blood samples were obtained from retro-orbital venous plexus at the 1st day then the 6th, 8th, 10th and 12th weeks for measuring blood glucose, serum creatinine and blood urea nitrogen (BUN). Serum level of creatinine and BUN were determined using an auto-analyzer (Hitachi 912 Auto-Analyzer; Hitachi, Japan). Fasting blood glucose was estimated by the glucose oxidase-peroxidase method (GOD-POD kit from Biodiagnostic, Egypt). Additionally, rats were located in metabolic cages for collection of 24h urine for measuring urinary albumin at the same intervals. Urinary protein excretion was determined using Fortress Diagnostics Limited Unit 2C Antrim Technology Park, Antrim BT41 1QS, United Kingdom.

Nephropathy was confirmed in rats at the end of the 6th week by the significant increase in protein in the urine, serum creatinine and BUN when compared with control. Rats having these significant values were enrolled in the study.

At the end of the 12th week, the rats were anesthetized by sodium thiopental anesthesia (40 mg/kg I.P.) after 12 hours of fasting. The rats were fixed on an operating table and the blood

Preprints (www.preprints.org) | NOT PEER-REVIEWED | Posted: 10 September 2018 doi:10.20944/preprints201809.0153.v1

samples were obtained from retro-orbital venous plexus using a fine-walled Pasteur pipette. Then vascular perfusion fixation through the left ventricle with 1% glutaraldehyde was performed. The kidneys were collected from rats of all groups for histological, immunohistochemical, transmission electron microscopy, qPCR study and western blot.

Histological analysis:

Light microscopic study:

The specimens were excised; paraffin sections of 4-6 µm thickness were performed and then mounted on glass slides for H & E and Masson's trichrome stains [64]. Immunohistochemistry staining for detection of transforming growth factor β (TGF-β). The primary monoclonal antibody used was rabbit monoclonal antibody to TGF-β (Lab Vision Corp, Neo-markers, Inc/Lab Vision, Fremont, California, USA). Positive reaction was detected as a brown color in the cytoplasm [65].

Transmission electron microscopic study (TEM):

Vascular perfusion fixation through the left ventricle with 1% glutaraldehyde was performed then the kidneys were dissected and 1 mm^3 kidney samples were taken in 0.1 M phosphate buffer solution (PBS) pH 7.4 at 4 ºC for 2h, then washed three times with PBS (10 minutes each). Samples were then post fixed in 1% osmic acid for 30 minutes then washed three times with PBS (10 minutes each). Samples were dehydrated with ascending series of ethyl alcohol (30, 50, 70, 90% and absolute alcohol) each concentration for 30 minutes. Samples were infiltrated with acetone for 1 hour and then embedded in Araldite 502 resin. The plastic molds were cut using LEICA Ultra cut (UCT ultra-microtome), stained with 1% toluidine blue. After examination of semi thin sections, ultra-thin sections (50-60 nm thick) were cut, stained with uranyl acetate, then counter

 doi:10.20944/preprints201809.0153.v1

stained with lead citrate, examined and photographed using JEOL-JEM-100 SX electron microscope, Japan, electron microscope unit, Tanta University [66].

Morphometric study:

The mean area percent of collagen fibers deposition by Masson's trichrome and the mean area percent of TGF-β expression were quantified in five images from five non-overlapping fields from each rat of each group using Image-Pro Plus program version 6.0 (Media Cybernetics Inc., Bethesda, Maryland, USA).

The expressions of *LC3*, *mTOR* and *Beclin 1* genes were determined by qPCR as follows:

Total RNA extraction and reverse transcription:

Total RNA was extracted from frozen Kidney tissue samples by Trizol method (Invitrogen, USA) using RNeasy mini kit (Qiagen, Germany) as previously described [67]. Samples were quantified using NanoDrop One spectrophotometer (Thermo Fisher Scientific, USA). RNA (1 µg) was reverse transcribed by T100 Thermal Cycler (Bio-Rad, USA) using Maxima First Strand cDNA Synthesis Kit (Thermo Fisher Scientific, USA), following the manufacturer's guidelines [68].

Quantitative real-time PCR:

Real-time PCR was performed according to manufacturer's instructions using Maxima SYBR Green/ROX qPCR Master Mix (Thermo Fisher, USA), by Step One Plus Real-Time PCR System (Life Technologies, USA) [69]. The primers sequences were as follows: **GAPDH forward**:

Preprints (www.preprints.org) | NOT PEER-REVIEWED | Posted: 10 September 2018 doi:10.20944/preprints201809.0153.v1

TGATTCTACCCACGGCAAGTT; **GAPDH reverse**: TGATGGGTTTCCCATTGATGA; **LC3-II forward**: ACTGCCGCCCTAAAGGTTAC; **LC3-II reverse**: CGAGGTCCAACCCACAAAGA; **Beclin-1 forward**: CGGCTCCTATTCCATCAAAA; **Beclin-1 reverse**: AACTGTGAGGACAC CCAAGC; [70] and **mTOR forward** TTGAGGTTGCTATGACCAGAGAGAA; **mTOR reverse** TTACCAGAAAGGACACCAGCCAATG [71]. The mRNA expression of each sample was determined after correction by *GAPDH* expression. The relative expression was calculated using the $2^{-\Delta\Delta CT}$ method. The results were expressed as the n-fold difference relative to the control group. Each sample was assayed three times.

Western blot

The mTOR, LC3-I, LC3-II, fibronectin, TGF-β and β-actin antibody used were purchased from **abcam** (Anti-Fibronectin antibody (ab23750), Rabbit polyclonalantibody [72], Anti-TGF beta 1 antibody (ab92486), Rabbit polyclonal antibody [73], Anti-LC3-I/II Antibody (ABC929, Sigma-Aldrich), Rabbit polyclonal antibody [74], Anti-mTOR antibody (ab2732), Rabbit polyclonal antibody [75]). The Proteins of renal tissues were extracted by RIPA lysis buffer which was delivered by Bio BASIC INC. (Marhham Ontario L3R 8T4 Canada). Extracted proteins were separated by SDS-PAGE on 4-20% polyacrylamide gradient gels. After incubation in 5% non-fat dry milk, Tris-HCL, 0.1% Tween 20 for 1 hr, primary antibodies (fibronectin, TGF-β, mTOR and LC3 II polyclonal antibodies) and β-actin antibody each were added to one of the membranes containing specimen samples and incubated at 4ºC overnight. Appropriate secondary antibodies were incubated for 2 hr at room temperature. After being washed twice with 1x TBST, densitometric analysis of the immunoblots were performed to quantify the amounts of collagen-I

 doi:10.20944/preprints201809.0153.v1

and β –actin against control sample by total protein normalization using Image analysis software on the Chemi Doc MP imaging system (Version 3) produced by Bio-Rad (Hercules, CA).

Statistical analysis:

A statistical analysis was performed using the statistical software package SPSS for Windows (Version 18.0; SPSS Inc., Chicago, IL, USA). Differences between groups were evaluated using a one-way ANOVA followed by *Duncan* post-hoc test. For each test, all the data are expressed as the mean ± standard error of mean (SE), and a P value <0.05 was considered significant.

Abbreviations:

3-MA: 3-methyladenine; BUN: blood urea nitrogen; DN: diabetic nephropathy; ESRD: end-stage renal disease; LC3: Microtubule-associated protein 1A/1B-light chain 3; MSCs: mesenchymal stem cells; mTOR: mechanistic target of rapamycin; STZ: Streptozotocin; TGF: Transforming growth factor; ULK1: Unc-51 like autophagy activating kinase

Declarations

Ethics approval and consent to participate

This study was carried out in strict accordance with the recommendations in the Guide for the Care and Use of Laboratory Animals of the National Institutes of Health (NIH publication No. 85–

 doi:10.20944/preprints201809.0153.v1

23, revised 2011). All protocols were approved by the institutional review board for animal experiments of the Faculty of Medicine, Benha University, Egypt.

Consent for publication

All authors agreed to publish this manuscript.

Availability of data and materials

All data generated and/or analyzed during this study are included in this published article.

Competing interests

The authors declare that they have no competing interests.

Funding

Disclosure of conflict of interest: None.

This research did not receive any specific grant from funding agencies in the public, commercial, or not-for-profit sectors.

Authors' contributions

NE, IAA, NIH, AAD, YS, SMS and ASF designed and planned the study. NE, DS, IAA, NIH, OM and ASF performed the experiments. NE, AMH, NIH, AME and AAD collected the data, and AAD, IAA, OM, NIH, AMH and ASF analyzed the data. NE, NIH, IAA and ASF were a major contributor in writing the manuscript. NE amended the manuscript. All authors read and approved the final manuscript.

 doi:10.20944/preprints201809.0153.v1

Acknowledgments

We would like to represent our acknowledgments for the research team of the Central Lab at Faculty of Medicine, Benha University and Molecular Biology Unit, Faculty of Medicine, Cairo University.

 doi:10.20944/preprints201809.0153.v1

References:

1. Martínez-Castelao A; Navarro-González JF; Górriz JL; de Alvaro F. The concept and the epidemiology of diabetic nephropathy have changed in recent years. *Journal of clinical medicine* **2015**, 4(6),1207-1216.
2. Saran R; Robinson B; Abbott KC; Agodoa LY; Albertus P; Ayanian J; Balkrishnan R; Bragg-Gresham J; Cao J; Chen JL. US renal data system 2016 annual data report: epidemiology of kidney disease in the United States. *American journal of kidney diseases* **2017**, 69(3),A7-A8.
3. Forbes JM; Coughlan MT; Cooper ME. Oxidative stress as a major culprit in kidney disease in diabetes. *Diabetes* **2008**, 57(6),1446-1454.
4. Lorenzen JM; Haller H; Thum T. MicroRNAs as mediators and therapeutic targets in chronic kidney disease. *Nature Reviews Nephrology* **2011**, 7(5),286.
5. Fernandez-Fernandez B; Ortiz A; Gomez-Guerrero C; Egido J. Therapeutic approaches to diabetic nephropathy—beyond the RAS. *Nature Reviews Nephrology* **2014**, 10(6),325.
6. Ahmad J. Management of diabetic nephropathy: recent progress and future perspective. *Diabetes & Metabolic Syndrome: Clinical Research & Reviews* **2015**, 9(4),343-358.
7. Satirapoj B; Adler SG. Comprehensive approach to diabetic nephropathy. *Kidney research and clinical practice* **2014**, 33(3),121-131.
8. Tögel F; Weiss K; Yang Y; Hu Z; Zhang P; Westenfelder C. Vasculotropic, paracrine actions of infused mesenchymal stem cells are important to the recovery from acute kidney injury. *American Journal of Physiology-Renal Physiology* **2007**, 292(5),F1626-F1635.
9. Ullah I; Subbarao RB; Rho GJ. Human mesenchymal stem cells-current trends and future prospective. *Bioscience reports* **2015**, 35(2),e00191.
10. Katsuda T; Kosaka N; Takeshita F; Ochiya T. The therapeutic potential of mesenchymal stem cell-derived extracellular vesicles. *Proteomics* **2013**, 13(10-11),1637-1653.
11. Roy S; Hochberg FH; Jones PS. Extracellular vesicles: the growth as diagnostics and therapeutics; a survey. *Journal of extracellular vesicles* **2018**, 7(1),1438720.
12. Yeagy BA; Cherqui S. Kidney repair and stem cells: a complex and controversial process. *Pediatric nephrology* **2011**, 26(9),1427-1434.

13. Zarjou A; Kim J; Traylor AM; Sanders PW; Balla J; Agarwal A; Curtis LM. Paracrine effects of mesenchymal stem cells in cisplatin-induced renal injury require heme oxygenase-1. *American journal of physiology Renal physiology* **2011**, 300(1),F254-262.
14. Chen Y; Qian H; Zhu W; Zhang X; Yan Y; Ye S; Peng X; Li W; Xu W. Hepatocyte growth factor modification promotes the amelioration effects of human umbilical cord mesenchymal stem cells on rat acute kidney injury. *Stem cells and development* **2010**, 20(1),103-113.
15. Johansen T; Lamark T. Selective autophagy mediated by autophagic adapter proteins. *Autophagy* **2011**, 7(3),279-296.
16. De Rechter S; Decuypere J-P; Ivanova E; van den Heuvel LP; De Smedt H; Levtchenko E; Mekahli D. Autophagy in renal diseases. *Pediatric nephrology* **2016**, 31(5),737-752.
17. Ding Y; Choi ME. Autophagy in diabetic nephropathy. *Journal of Endocrinology* **2014**,JOE-14-0437.
18. Deng X; Xie Y; Zhang A. Advance of autophagy in chronic kidney diseases. *Renal failure* **2017**, 39(1),306-313.
19. Zoncu R; Efeyan A; Sabatini DM. mTOR: from growth signal integration to cancer, diabetes and ageing. *Nature reviews Molecular cell biology* **2011**, 12(1),21.
20. Lloberas N; Cruzado JM; Franquesa M; Herrero-Fresneda I; Torras J; Alperovich G; Rama I; Vidal A; Grinyó JM. Mammalian target of rapamycin pathway blockade slows progression of diabetic kidney disease in rats. *Journal of the American Society of Nephrology* **2006**, 17(5),1395-1404.
21. Mori H; Inoki K; Masutani K; Wakabayashi Y; Komai K; Nakagawa R; Guan K-L; Yoshimura A. The mTOR pathway is highly activated in diabetic nephropathy and rapamycin has a strong therapeutic potential. *Biochemical and biophysical research communications* **2009**, 384(4),471-475.
22. Gödel M; Hartleben B; Herbach N; Liu S; Zschiedrich S; Lu S; Debreczeni-Mór A; Lindenmeyer MT; Rastaldi M-P; Hartleben G. Role of mTOR in podocyte function and diabetic nephropathy in humans and mice. *The Journal of clinical investigation* **2011**, 121(6),2197-2209.
23. Thomas MC; Cooper ME; Zimmet P. Changing epidemiology of type 2 diabetes mellitus and associated chronic kidney disease. *Nature Reviews Nephrology* **2016**, 12(2),73.

24. Mokdad AH; Ford ES; Bowman BA; Dietz WH; Vinicor F; Bales VS; Marks JS. Prevalence of obesity, diabetes, and obesity-related health risk factors, 2001. *Jama* **2003**, 289(1),76-79.

25. Tanaka Y; Kume S; Kitada M; Kanasaki K; Uzu T; Maegawa H; Koya D. Autophagy as a therapeutic target in diabetic nephropathy. *Experimental diabetes research* **2011**, 2012.

26. Matboli M; Eissa S; Ibrahim D; Hegazy MG; Imam SS; Habib EK. Caffeic acid attenuates diabetic kidney disease via modulation of autophagy in a high-fat diet/streptozotocin-induced diabetic rat. *Scientific Reports* **2017**, 7(1),2263.

27. Abou-Hany HO; Atef H; Said E; Elkashef HA; Salem HA. Crocin mediated amelioration of oxidative burden and inflammatory cascade suppresses diabetic nephropathy progression in diabetic rats. *Chemico-biological interactions* **2018**, 284,90-100.

28. Duan P; Hu C; Quan C; Yu T; Huang W; Chen W; Tang S; Shi Y; Martin FL; Yang K. 4-Nonylphenol induces autophagy and attenuates mTOR-p70S6K/4EBP1 signaling by modulating AMPK activation in Sertoli cells. *Toxicology letters* **2017**, 267,21-31.

29. Hsieh C-Y; Miaw C-L; Hsieh C-C; Tseng H-C; Yang Y-H; Yen C-H. Effects of chronic 4-n-nonylphenol treatment on aortic vasoconstriction and vasorelaxation in rats. *Archives of toxicology* **2009**, 83(10),941-946.

30. Malik A; Mehmood MH; Channa H; Akhtar MS; Gilani A-H. Pharmacological basis for the medicinal use of polyherbal formulation and its ingredients in cardiovascular disorders using rodents. *BMC complementary and alternative medicine* **2017**, 17(1),142.

31. Kriz W; Lemley KV. Mechanical challenges to the glomerular filtration barrier: adaptations and pathway to sclerosis. *Pediatric nephrology* **2017**, 32(3),405-417.

32. Swiatecka-Urban A. Endocytic trafficking at the mature podocyte slit diaphragm. *Frontiers in pediatrics* **2017**, 5,32.

33. Cara-Fuentes G; Clapp WL; Johnson RJ; Garin EH. Pathogenesis of proteinuria in idiopathic minimal change disease: molecular mechanisms. *Pediatric nephrology* **2016**, 31(12),2179-2189.

34. Lenoir O; Jasiek M; Hénique C; Guyonnet L; Hartleben B; Bork T; Chipont A; Flosseau K; Bensaada I; Schmitt A. Endothelial cell and podocyte autophagy synergistically protect from diabetes-induced glomerulosclerosis. *Autophagy* **2015**, 11(7),1130-1145.

35. Kang R; Zeh H; Lotze M; Tang D. The Beclin 1 network regulates autophagy and apoptosis. *Cell death and differentiation* **2011**, 18(4),571.

36. Klionsky DJ; Abdelmohsen K; Abe A; Abedin MJ; Abeliovich H; Acevedo Arozena A; Adachi H; Adams CM; Adams PD; Adeli K. Guidelines for the use and interpretation of assays for monitoring autophagy. *Autophagy* **2016**, 12(1),1-222.

37. Fang L; Zhou Y; Cao H; Wen P; Jiang L; He W; Dai C; Yang J. Autophagy attenuates diabetic glomerular damage through protection of hyperglycemia-induced podocyte injury. *PloS one* **2013**, 8(4),e60546.

38. Godel M; Hartleben B; Herbach N; Liu S; Zschiedrich S; Lu S; Debreczeni-Mor A; Lindenmeyer MT; Rastaldi MP; Hartleben G *et al*. Role of mTOR in podocyte function and diabetic nephropathy in humans and mice. *J Clin Invest* **2011**, 121(6),2197-2209.

39. Liu WJ; Huang WF; Ye L; Chen RH; Yang C; Wu HL; Pan QJ; Liu HF. The activity and role of autophagy in the pathogenesis of diabetic nephropathy. *Eur Rev Med Pharmacol Sci* **2018**, 22(10),3182-3189.

40. Lee C-H; Inoki K; Guan K-L. mTOR pathway as a target in tissue hypertrophy. *Annu Rev Pharmacol Toxicol* **2007**, 47,443-467.

41. Chen J-K; Chen J; Neilson EG; Harris RC. Role of mammalian target of rapamycin signaling in compensatory renal hypertrophy. *Journal of the American Society of Nephrology* **2005**, 16(5),1384-1391.

42. Yang Y; Wang J; Qin L; Shou Z; Zhao J; Wang H; Chen Y; Chen J. Rapamycin prevents early steps of the development of diabetic nephropathy in rats. *American journal of nephrology* **2007**, 27(5),495-502.

43. Inoki K; Mori H; Wang J; Suzuki T; Hong S; Yoshida S; Blattner SM; Ikenoue T; Rüegg MA; Hall MN. mTORC1 activation in podocytes is a critical step in the development of diabetic nephropathy in mice. *The Journal of clinical investigation* **2011**, 121(6),2181-2196.

44. Gonzalez CD; Lee M-S; Marchetti P; Pietropaolo M; Towns R; Vaccaro MI; Watada H; Wiley JW. The emerging role of autophagy in the pathophysiology of diabetes mellitus. *Autophagy* **2011**, 7(1),2-11.

45. Yamahara K; Kume S; Koya D; Tanaka Y; Morita Y; Chin-Kanasaki M; Araki H; Isshiki K; Araki S-i; Haneda M. Obesity-mediated autophagy insufficiency exacerbates

proteinuria-induced tubulointerstitial lesions. *Journal of the American Society of Nephrology* **2013**,ASN. 2012111080.

46. Peng KY; Horng LY; Sung HC; Huang HC; Wu RT. Hepatocyte growth factor has a role in the amelioration of diabetic vascular complications via autophagic clearance of advanced glycation end products: Dispo85E, an HGF inducer, as a potential botanical drug. *Metabolism: clinical and experimental* **2011**, 60(6),888-892.
47. Ding Y; Choi ME. Autophagy in diabetic nephropathy. *The Journal of endocrinology* **2015**, 224(1),R15-30.
48. Tanaka Y; Kume S; Kitada M; Kanasaki K; Uzu T; Maegawa H; Koya D. Autophagy as a therapeutic target in diabetic nephropathy. *Exp Diabetes Res* **2012**, 2012,628978.
49. Mizushima N. The role of the Atg1/ULK1 complex in autophagy regulation. *Current opinion in cell biology* **2010**, 22(2),132-139.
50. Nagaishi K; Mizue Y; Chikenji T; Otani M; Nakano M; Konari N; Fujimiya M. Mesenchymal stem cell therapy ameliorates diabetic nephropathy via the paracrine effect of renal trophic factors including exosomes. *Scientific reports* **2016**, 6,34842.
51. Nassar W; El-Ansary M; Sabry D; Mostafa MA; Fayad T; Kotb E; Temraz M; Saad AN; Essa W; Adel H. Umbilical cord mesenchymal stem cells derived extracellular vesicles can safely ameliorate the progression of chronic kidney diseases. *Biomaterials research* **2016**, 20,21.
52. Bruno S; Grange C; Collino F; Deregibus MC; Cantaluppi V; Biancone L; Tetta C; Camussi G. Microvesicles derived from mesenchymal stem cells enhance survival in a lethal model of acute kidney injury. *PloS one* **2012**, 7(3),e33115.
53. Nagaishi K; Mizue Y; Chikenji T; Otani M; Nakano M; Konari N; Fujimiya M. Mesenchymal stem cell therapy ameliorates diabetic nephropathy via the paracrine effect of renal trophic factors including exosomes. *Sci Rep* **2016**, 6,34842.
54. Liu L; Jin X; Hu CF; Li R; Zhou Z; Shen CX. Exosomes Derived from Mesenchymal Stem Cells Rescue Myocardial Ischaemia/Reperfusion Injury by Inducing Cardiomyocyte Autophagy Via AMPK and Akt Pathways. *Cellular physiology and biochemistry : international journal of experimental cellular physiology, biochemistry, and pharmacology* **2017**, 43(1),52-68.

55. Mu Y; Yan WJ; Yin TL; Zhang Y; Li J; Yang J. Diet-induced obesity impairs spermatogenesis: a potential role for autophagy. *Sci Rep* **2017**, 7,43475.

56. Tang Y; Cai QH; Wang YJ; Fan SH; Zhang ZF; Xiao MQ; Zhu JY; Wu DM; Lu J; Zheng YL. Protective effect of autophagy on endoplasmic reticulum stress induced apoptosis of alveolar epithelial cells in rat models of COPD. *Biosci Rep* **2017**, 37(6).

57. Wu YT; Tan HL; Shui G; Bauvy C; Huang Q; Wenk MR; Ong CN; Codogno P; Shen HM. Dual role of 3-methyladenine in modulation of autophagy via different temporal patterns of inhibition on class I and III phosphoinositide 3-kinase. *The Journal of biological chemistry* **2010**, 285(14),10850-10861.

58. Verschooten L; Barrette K; Van Kelst S; Rubio Romero N; Proby C; De Vos R; Agostinis P; Garmyn M. Autophagy inhibitor chloroquine enhanced the cell death inducing effect of the flavonoid luteolin in metastatic squamous cell carcinoma cells. *PLoS One* **2012**, 7(10),e48264.

59. Gatti S; Bruno S; Deregibus MC; Sordi A; Cantaluppi V; Tetta C; Camussi G. Microvesicles derived from human adult mesenchymal stem cells protect against ischaemia–reperfusion-induced acute and chronic kidney injury. *Nephrology Dialysis Transplantation* **2011**, 26(5),1474-1483.

60. Yang J; Liu X-X; Fan H; Tang Q; Shou Z-X; Zuo D-M; Zou Z; Xu M; Chen Q-Y; Peng Y. Extracellular vesicles derived from bone marrow mesenchymal stem cells protect against experimental colitis via attenuating colon inflammation, oxidative stress and apoptosis. *PLoS One* **2015**, 10(10),e0140551.

61. Lange-Consiglio A; Perrini C; Albini G; Modina S; Lodde V; Orsini E; Esposti P; Cremonesi F. Oviductal microvesicles and their effect on in vitro maturation of canine oocytes. *Reproduction* **2017**, 154(2),167-180.

62. Tesch GH; Allen TJ. Rodent models of streptozotocin-induced diabetic nephropathy (Methods in Renal Research). *Nephrology* **2007**, 12(3),261-266.

63. Tang Y; Cai Q-H; Wang Y-J; Fan S-H; Zhang Z-F; Xiao M-Q; Zhu J-Y; Wu D-M; Lu J; Zheng Y-L. Protective effect of autophagy on endoplasmic reticulum stress-induced apoptosis of alveolar epithelial cells in rat models of COPD. *Bioscience reports* **2017**,BSR20170803.

64. Hayat MA: Principles and techniques of electron microscopy. Biological applications: Edward Arnold.; 1981.

65. Yang B; El Nahas AM; Thomas GL; Haylor JL; Watson PF; Wagner B; Johnson TS. Caspase-3 and apoptosis in experimental chronic renal scarring. *Kidney international* **2001**, 60(5),1765-1776.

66. Wiame I; Remy S; Swennen R; Sagi L. Irreversible heat inactivation of DNase I without RNA degradation. *BioTechniques* **2000**, 29(2),252-256.

67. Wiame I; Remy S; Swennen R; Sagi L. Irreversible heat inactivation of DNase I without RNA degradation. *BioTechniques* **2000**, 29(2),252-254, 256.

68. Fleige S; Pfaffl MW. RNA integrity and the effect on the real-time qRT-PCR performance. *Molecular aspects of medicine* **2006**, 27(2-3),126-139.

69. Xu JT; Zhao X; Yaster M; Tao YX. Expression and distribution of mTOR, p70S6K, 4E-BP1, and their phosphorylated counterparts in rat dorsal root ganglion and spinal cord dorsal horn. *Brain Res* **2010**, 1336,46-57.

70. Wang X; Zhou G; Liu C; Wei R; Zhu S; Xu Y; Wu M; Miao Q. Acanthopanax versus 3-Methyladenine Ameliorates Sodium Taurocholate-Induced Severe Acute Pancreatitis by Inhibiting the Autophagic Pathway in Rats. *Mediators of Inflammation* **2016**, 2016,12.

71. Xu J-T; Zhao X; Yaster M; Tao Y-X. Expression and distribution of mTOR, p70S6K, 4E-BP1, and their phosphorylated counterparts in rat dorsal root ganglion and spinal cord dorsal horn. *Brain research* **2010**, 1336,46-57.

72. Cao X; Wang Y; Wu C; Li X; Fu Z; Yang M; Bian W; Wang S; Song Y; Tang J. Cathelicidin-OA1, a novel antioxidant peptide identified from an amphibian, accelerates skin wound healing. *Scientific reports* **2018**, 8(1),943.

73. Magalhaes J; Gegg M; Migdalska-Richards A; Schapira A. Effects of ambroxol on the autophagy-lysosome pathway and mitochondria in primary cortical neurons. *Scientific reports* **2018**, 8(1),1385.

74. Qian G; Liu D; Hu J; Gan F; Hou L; Zhai N; Chen X; Huang K. SeMet attenuates OTA-induced PCV2 replication promotion by inhibiting autophagy by activating the AKT/mTOR signaling pathway. *Veterinary research* **2018**, 49(1),15.

75. Kitada M; Takeda A; Nagai T; Ito H; Kanasaki K; Koya D. Dietary restriction ameliorates diabetic nephropathy through anti-inflammatory effects and regulation of the autophagy

 doi:10.20944/preprints201809.0153.v1

via restoration of Sirt1 in diabetic Wistar fatty (fa/fa) rats: a model of type 2 diabetes. *Experimental diabetes research* **2011**, 2011.

Preprints (www.preprints.org) | NOT PEER-REVIEWED | Posted: 10 September 2018 doi:10.20944/preprints201809.0153.v1

Legends:

Figure 1: Experimental design and treatment procedure. Rats were divided into five groups: Group I (Control group; *n*=21 subdivided into 3 subgroups [7 rats each]), Group II (DN group; *n*=14 subdivided into 2 groups [7 rats each]), Group III (DN+3-MA&Chloroquine; *n*=7), Group IV (DN+exosomes; *n*=7) and Group V (DN+3-MA&Chloroquine+exosomes; *n*=7)**.** Rats of DN groups were injected with STZ without/with treatment by3-MA&Chloroquine, exosome or both. On 1st day, weeks 6th, 8th, 10th and 12th blood samples were collected from all rats for biochemical assays, while on weeks 8th and 12th renal tissues were collected for histological, and molecular biological examinations.

Figure 2: TEM of exosomes showed spheroid double membrane bound morphology (arrows) with a diameter of 40-100 nm (A). Exosomes were also detected in renal tissues by PKH26 (B). Western blot for exosomes characterization (C). Histogram for exosomes characterization (D); Different superscripts (a, b and c) in the same column indicate significant differences at $P<0.05$. Data are shown as mean ± S.E.M, n = 5.

Figure 3: Blood glucose (a), serum urea (b) and BUN (c) as well as urinary proteins (d) from different experimental groups. Different superscripts (a, b, c and d) at the same checkpoint indicate significant differences at $P<0.05$. Data are shown as mean ± S.E.M, n = 7.

Preprints (www.preprints.org) | NOT PEER-REVIEWED | Posted: 10 September 2018 doi:10.20944/preprints201809.0153.v1

Figure 4: H&E stained sections of renal tissue of Group I **(A)** showed normal glomerulus (G) and tubules (T). Group IIa **(B)** showed mesangial expansion in the glomeruli (G) and glomerular nodular sclerosis (double arrows). Tubules (T) possess obliterated lumens and darkly stained nuclei with loss of nuclear polarity. Groups IIb & III **(C&D)** demonstrated shrunken glomeruli (G) with wide Bowman's spaces (thin arrows). The tubules (T) possess swollen epithelial lining obliterating the lumens in addition to darkly staining nuclei with loss of their polarity. Group IV **(E)** revealed decreased mesangial expansion in the glomeruli (G). Tubules (T) have open lumens and normal nuclear polarity. Group IV **(F)** showed persistent mesangial expansion in the glomeruli (G), swollen tubular epithelia (T) obliterating the lumens and darkly stained nuclei with loss of their polarity. **(H&E X400)**

Figure 5: Masson's trichrome stained sections of renal cortex of Group I **(A)** showed minimal collagen fibers among the glomerular capillaries (arrow head) and surrounding the renal corpuscles and tubules (thin arrows). Group IIa **(B)** demonstrated accumulation of collagen fibers among the glomerular capillaries (arrow heads) and surrounding the renal corpuscles and tubules (thin arrows). Group IIb (**C**) showed marked accumulations of collagen fibers among the glomerular capillaries (arrow heads) and surrounding the renal corpuscles and tubules (thin arrows). Group III (**D**) showed extensive accumulations of collagen fibers among the glomerular capillaries (arrow head) and surrounding the renal corpuscles and tubules (thin arrows). Group IV **(E)** has few collagen fibers among the glomerular capillaries (arrow head) and around the renal corpuscles and tubules (thin arrows). Group V (**F**) demonstrated persistent accumulation of collagen fibers among the glomerular capillaries (arrow head) and surrounding the renal corpuscles and tubules (thin

Preprints (www.preprints.org) | NOT PEER-REVIEWED | Posted: 10 September 2018 doi:10.20944/preprints201809.0153.v1

arrows). A histogram **(G)** represented the mean area percentage of collagen fibers deposition in all experimental groups. **(Masson's trichrome X400).**

Figure 6: Immunohistochemical reaction for TGF-β in sections of the renal cortex of Group I **(A)** showed mild positive cytoplasmic reaction in the tubular epithelial cells (thin arrows). Group IIa **(B)** showed tubular cells with a moderate positive cytoplasmic reaction (thin arrows). Group IIb **(C)** presented a strong positive reaction in the cytoplasm of the tubular cells (thin arrows). Group III (**D**) displayed intense positive reactions in the cytoplasm of the tubular cells (thin arrows). Group IV **(E)** showed a mild positive cytoplasmic reaction (thin arrows). Group V **(F)**: tubular cells showing a moderate positive cytoplasmic reaction (thin arrows). A histogram **(G)** represented the mean area percentage of TGF-β immunoreaction in all experimental groups. **(Immunohistochemical reaction for TGF-β with hematoxylin as a counter stain X400)**

Figure 7: Ultrathin sections showing the glomerular filtration barriers of Group I **(A)** consisted of thin fenestrated (arrow head) endothelial cell **(E)**, thin regular glomerular basement membrane (curved arrow) and the foot processes of the podocytes (short arrow). Group IIa **(B)** showed extensive fusion and effacement of the foot processes (short arrows) and diffuse thickening of the glomerular basement membrane (curved arrows). Group IIb **(C)** with complete fusion and effacement of the foot processes (short arrows) and thickened glomerular basement membrane (curved arrows). Group III **(D)** showed areas of fusion and effacement of the podocytes (thin arrows) and diffuse thickening of the glomerular basement membrane (curved arrow). A vacuole (v) is seen compressing the nucleus of the endothelial cell. Group IV **(E)** with thin regular

Preprints (www.preprints.org) | NOT PEER-REVIEWED | Posted: 10 September 2018 doi:10.20944/preprints201809.0153.v1

glomerular basement membrane (curved arrow) and foot processes of podocytes (thin arrow). Group IV **(F)** revealed persistent fusion and effacement of the foot processes (short arrows) and thickening of the glomerular basement membrane (curved arrows) in some areas. **(TEM x 6000)**

Figure 8: Ultrathin sections showing the proximal tubular cells of Group I **(A)** resting on a thin regular basement membrane (thin arrow). Apical microvilli (mv) are numerous and tightly packed. Nucleus (N) appears oval and euchromatic and the cytoplasm contains numerous mitochondria (m). Group IIa **(B)** with a slightly thickened tubular basement membrane (thin arrow), swollen disrupted apical microvilli (mv) and shrunken nucleus (N). The cytoplasm shows areas of rarefaction (white arrows), numerous swollen mitochondria (m) and scattered electron dense bodies (d). Group IIb **(C)** with increased thickening of the tubular basement membrane (thin arrow), disrupted apical microvilli (mv) and a shrunken heterochromatic nucleus (N). The cytoplasm shows multiple variable sized vacuoles (v), variable sized mitochondria (m) and few scattered electron dense bodies (d). Group III **(D)** with a tubular cell resting on thickened basement membrane (thin arrow). Apical microvilli (mv) appear swollen and distorted. The nucleus (N) shows clumps of heterochromatin. The cytoplasm contains numerous swollen mitochondria (m) of various shapes and sizes. A small electron dense body (d) is also observed. Thin collagen fibrils (f) are seen in the interstitium. Group IV **(E)** showed proximal tubular cells resting on a thin basement membrane (thin arrow). The apical microvilli (mv) appear numerous and tightly packed and the nucleus (N) is round and euchromatic. The cytoplasm contains numerous autophagosomes (red arrows) containing cellular debris, numerous scattered electron dense bodies (d) and elongated mitochondria (m). Group V **(F)** shows persistent thickening of the tubular basement membrane in some areas (thin arrow), swollen apical microvilli (mv) and slightly shrunken nucleus (N). The

 doi:10.20944/preprints201809.0153.v1

cytoplasm shows areas of rarefication (white arrows), variable sized mitochondria (m) and scattered electron dense bodies (d). (**TEM x 6000**)

Figure 9: Quantitative analysis for relative LC3II, mTOR and Beclin 1 genes expression after the indicated treatment with 3-MA&Chloroquine and/or exosomes. Different superscripts (a, b and c) in the same column indicate significant differences at $P<0.05$. Data are shown as mean ± S.E.M, $n = 5$.

Figure 10: Western blot assay and downstream target proteins for mTOR, LC3-I, LC3-II, fibronectin, TGF-β and β-actin expression after treatment with 3-MA&Chloroquine and/or exosomes and quantified using Image analysis software on the Chemi Doc MP imaging system (A). Histogram for blotting intensity (B); Different superscripts (a, b and c) in the same column indicate significant differences at $P<0.05$. Data are shown as mean ± S.E.M, $n = 5$.

Preprints (www.preprints.org) | NOT PEER-REVIEWED | Posted: 10 September 2018 doi:10.20944/preprints201809.0153.v1

Figure 1

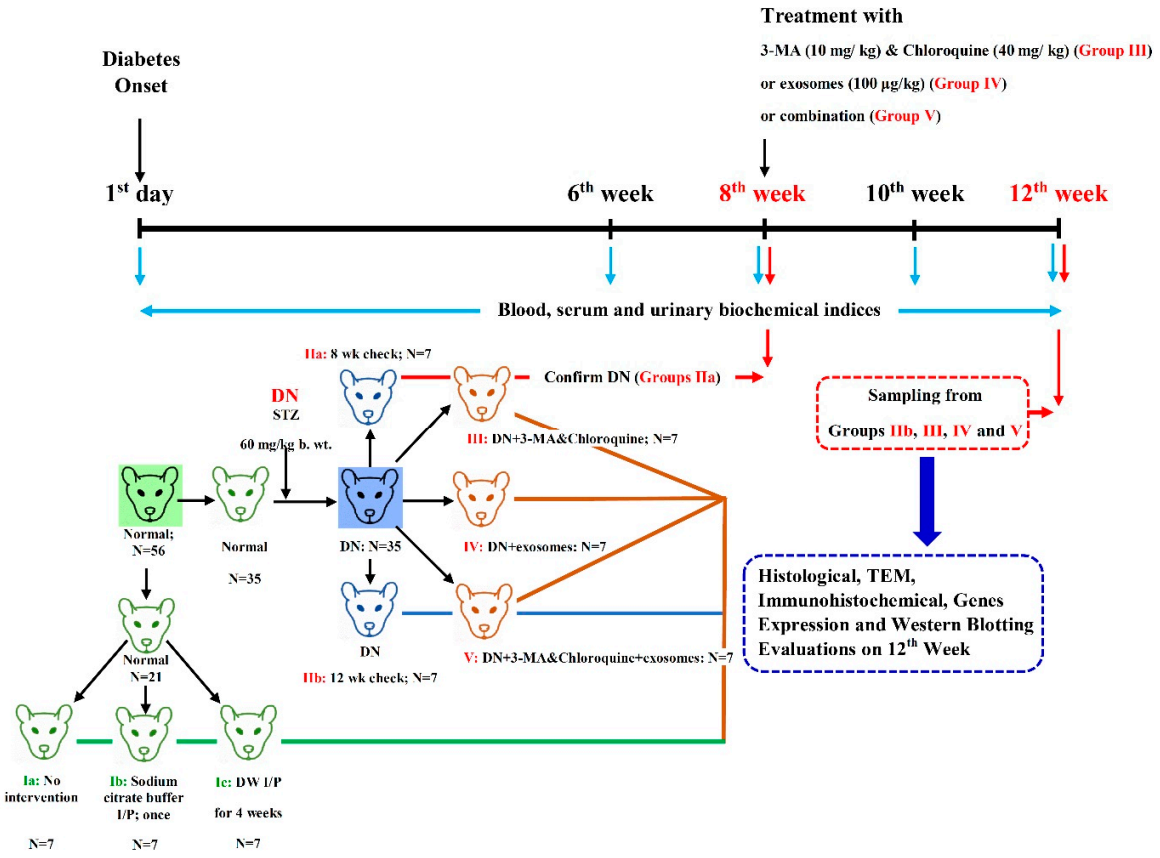

Preprints (www.preprints.org) | NOT PEER-REVIEWED | Posted: 10 September 2018 doi:10.20944/preprints201809.0153.v1

Figure 2

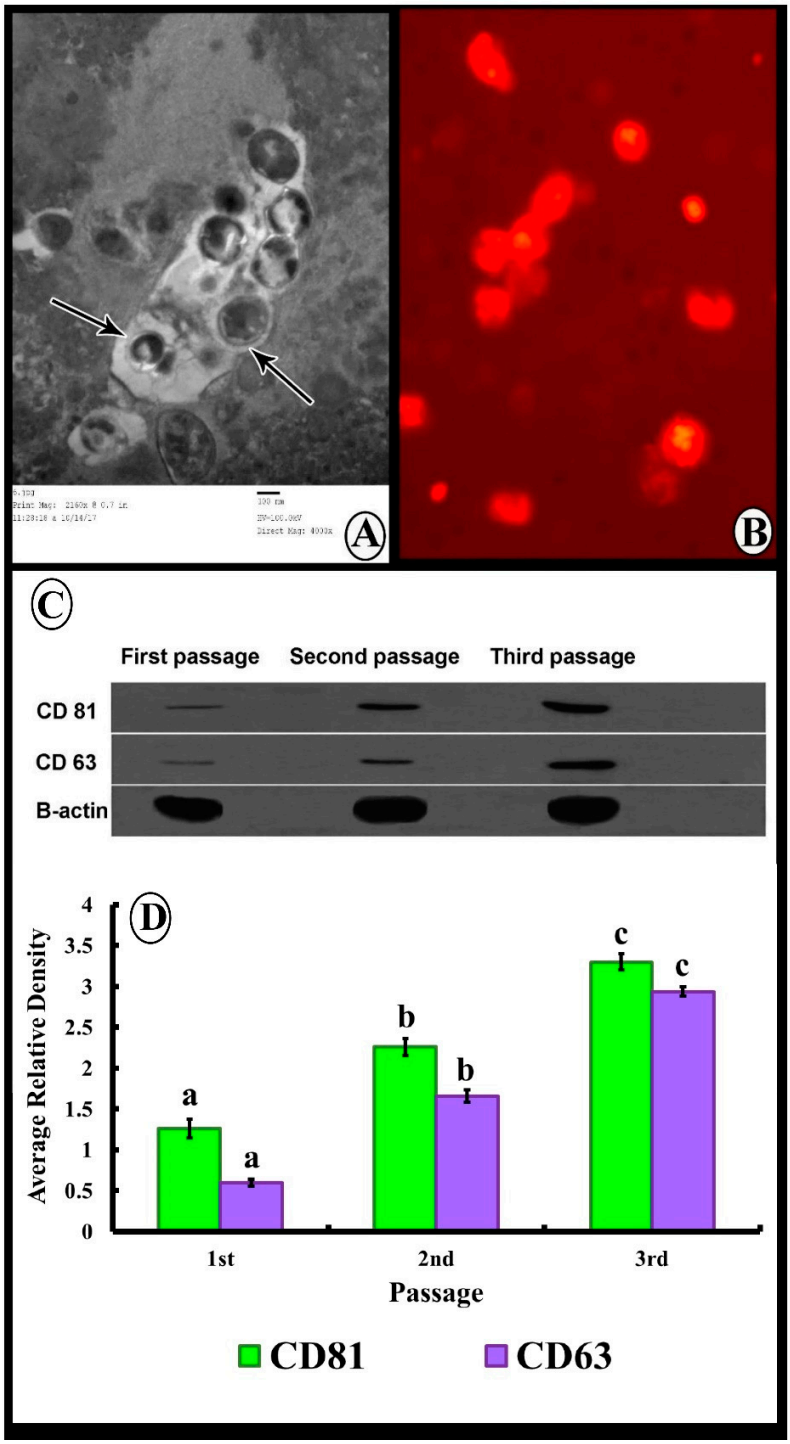

Preprints (www.preprints.org) | NOT PEER-REVIEWED | Posted: 10 September 2018 doi:10.20944/preprints201809.0153.v1

Figure 3

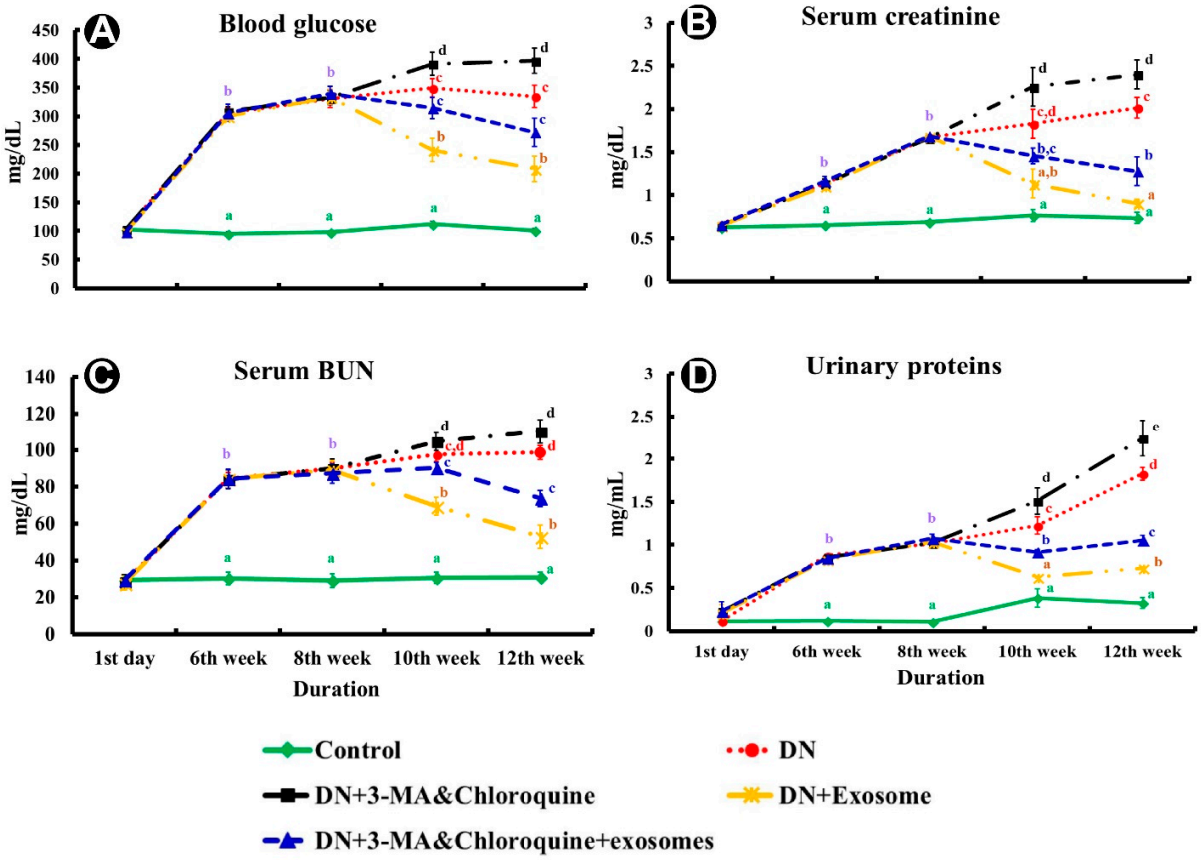

Preprints (www.preprints.org) | NOT PEER-REVIEWED | Posted: 10 September 2018 doi:10.20944/preprints201809.0153.v1

Figure 4

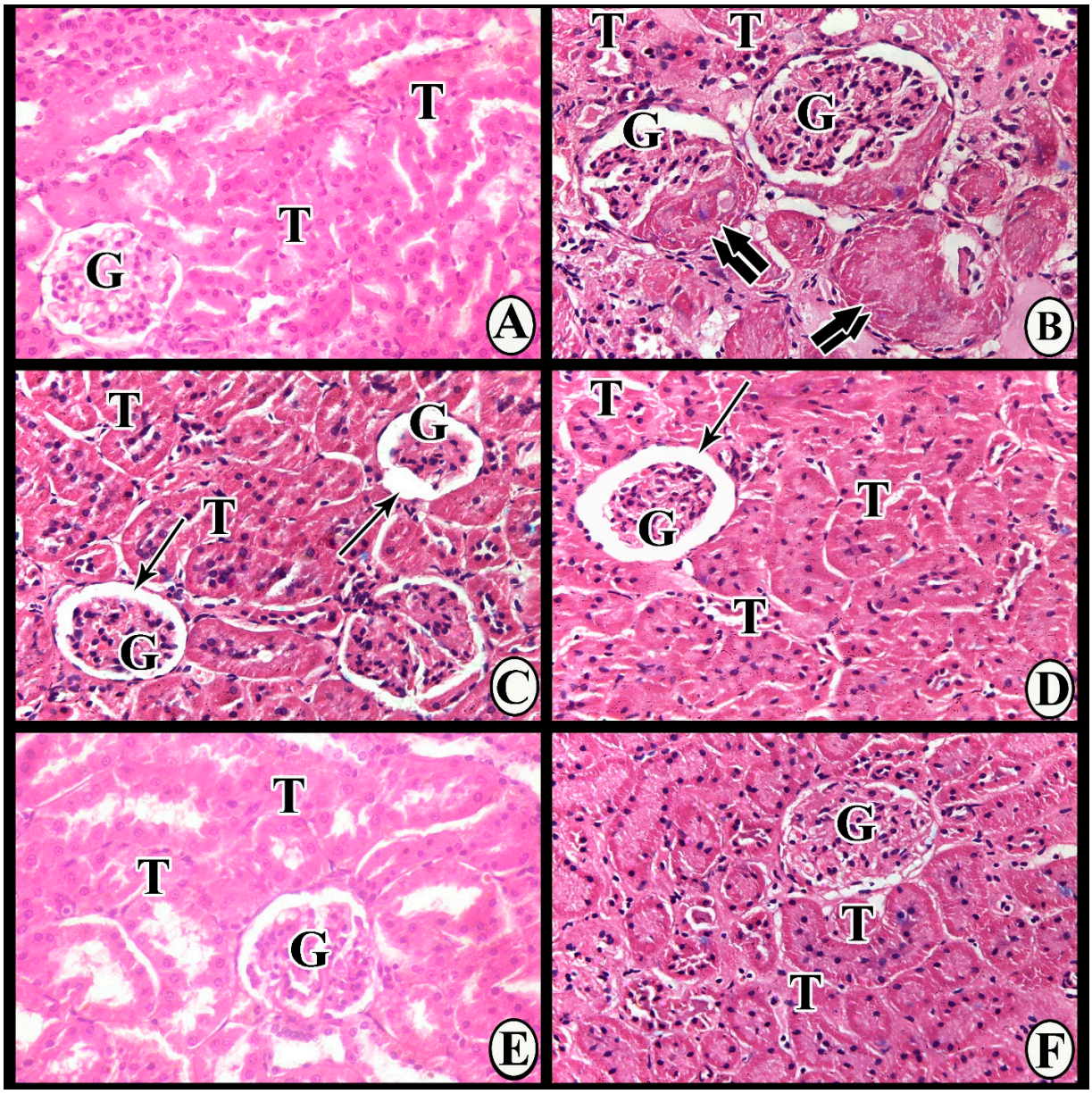

Preprints (www.preprints.org) | NOT PEER-REVIEWED | Posted: 10 September 2018 doi:10.20944/preprints201809.0153.v1

Figure 5

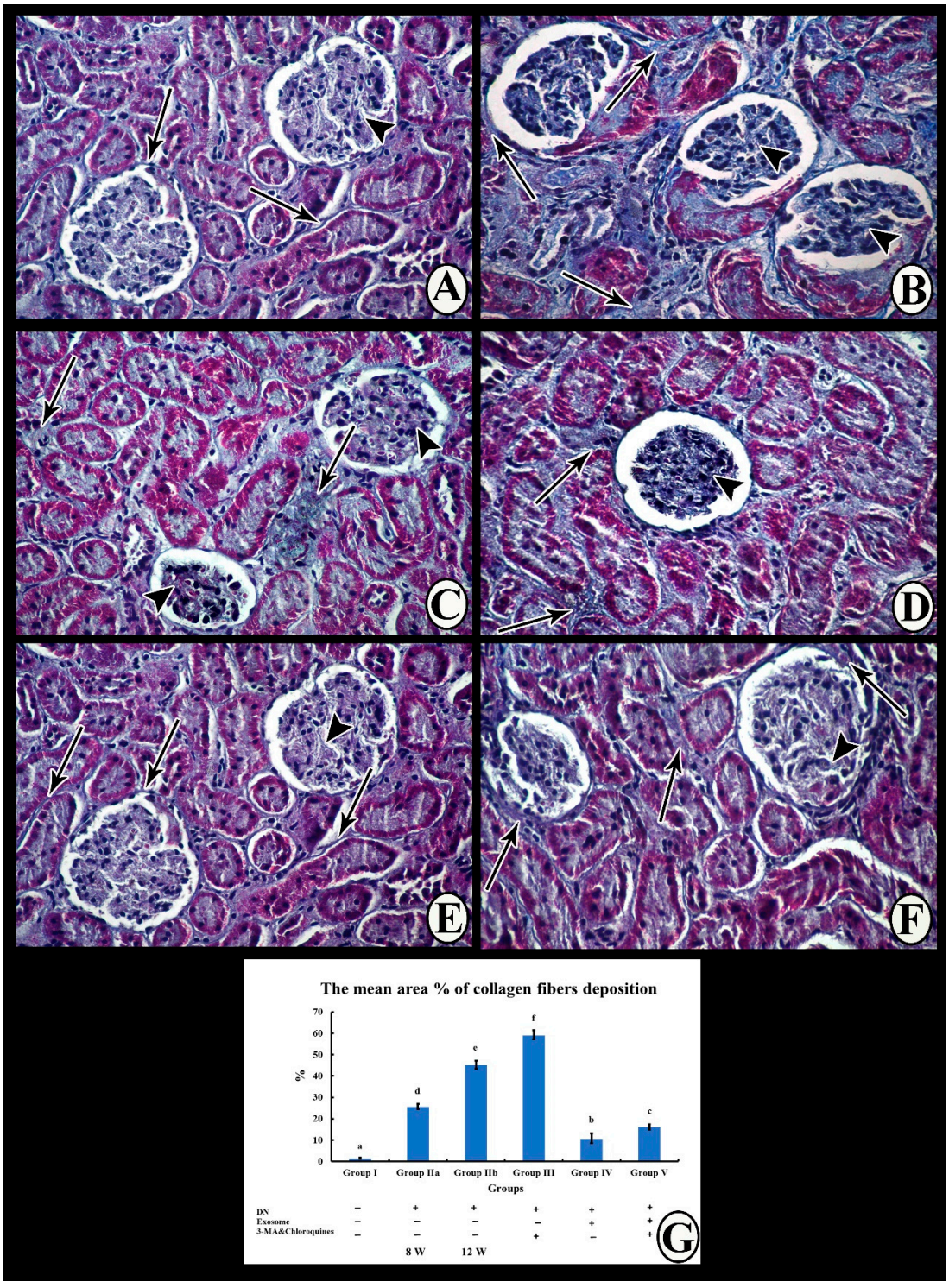

Preprints (www.preprints.org) | NOT PEER-REVIEWED | Posted: 10 September 2018 doi:10.20944/preprints201809.0153.v1

Figure 6

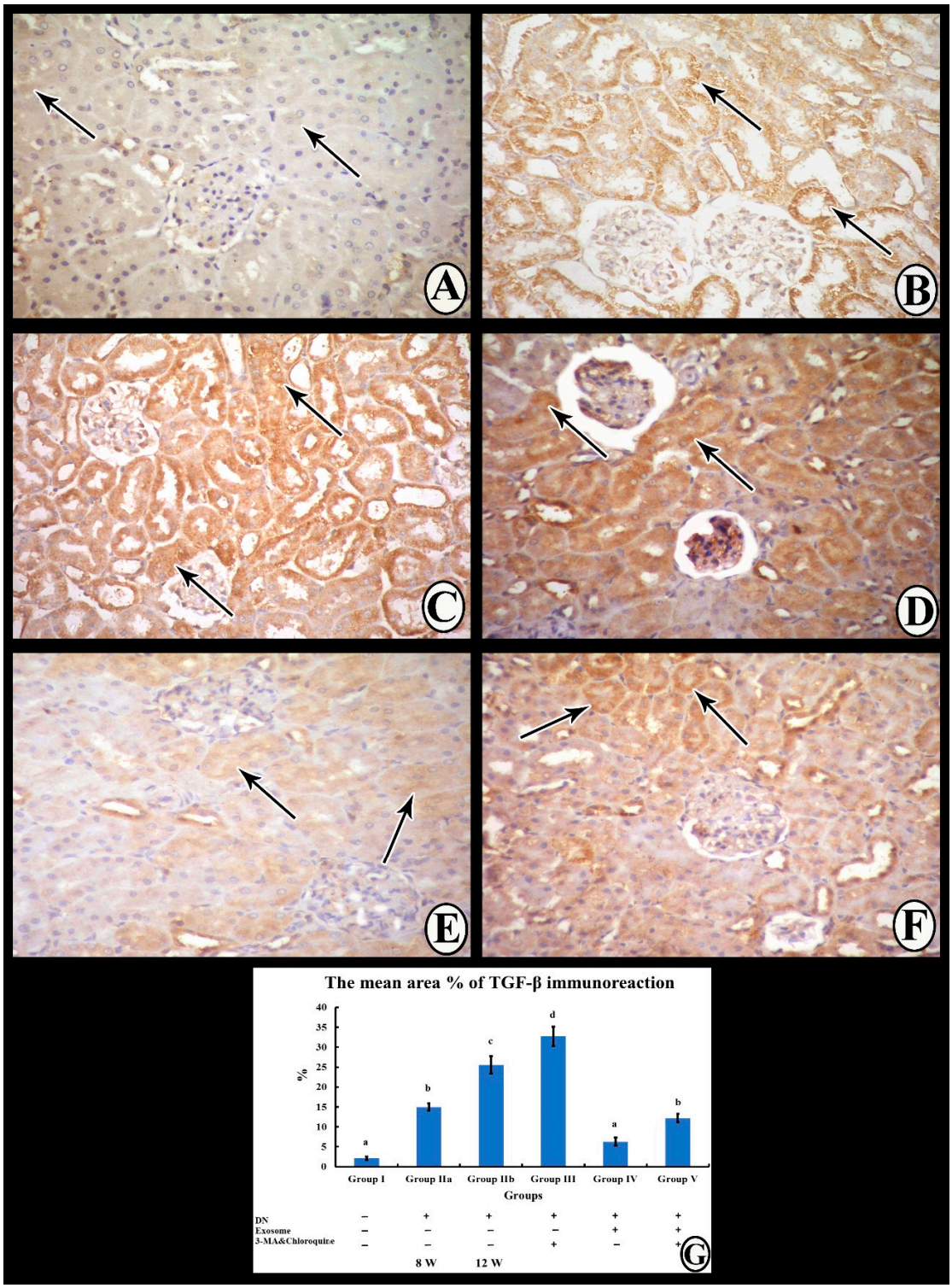

Preprints (www.preprints.org) | NOT PEER-REVIEWED | Posted: 10 September 2018 doi:10.20944/preprints201809.0153.v1

Figure 7

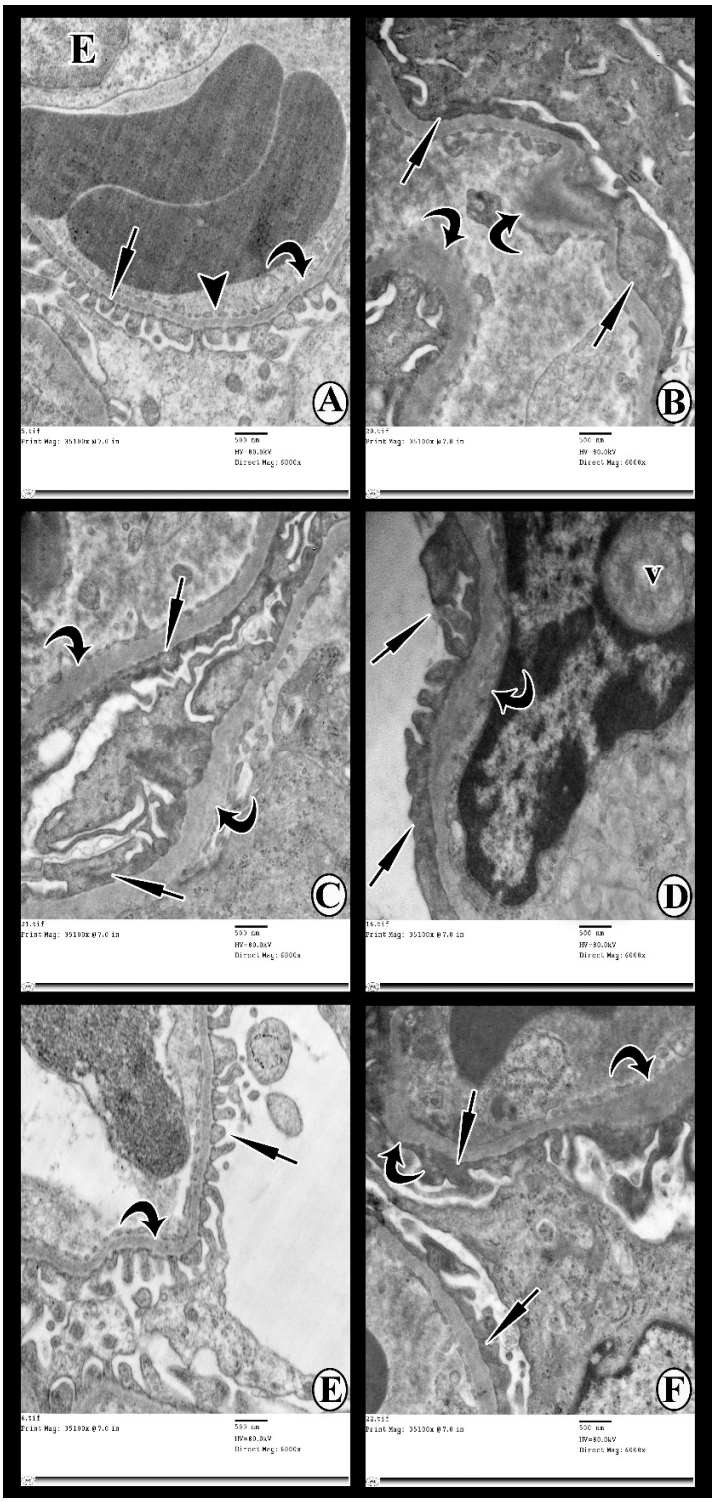

Preprints (www.preprints.org) | NOT PEER-REVIEWED | Posted: 10 September 2018 doi:10.20944/preprints201809.0153.v1

Figure 8

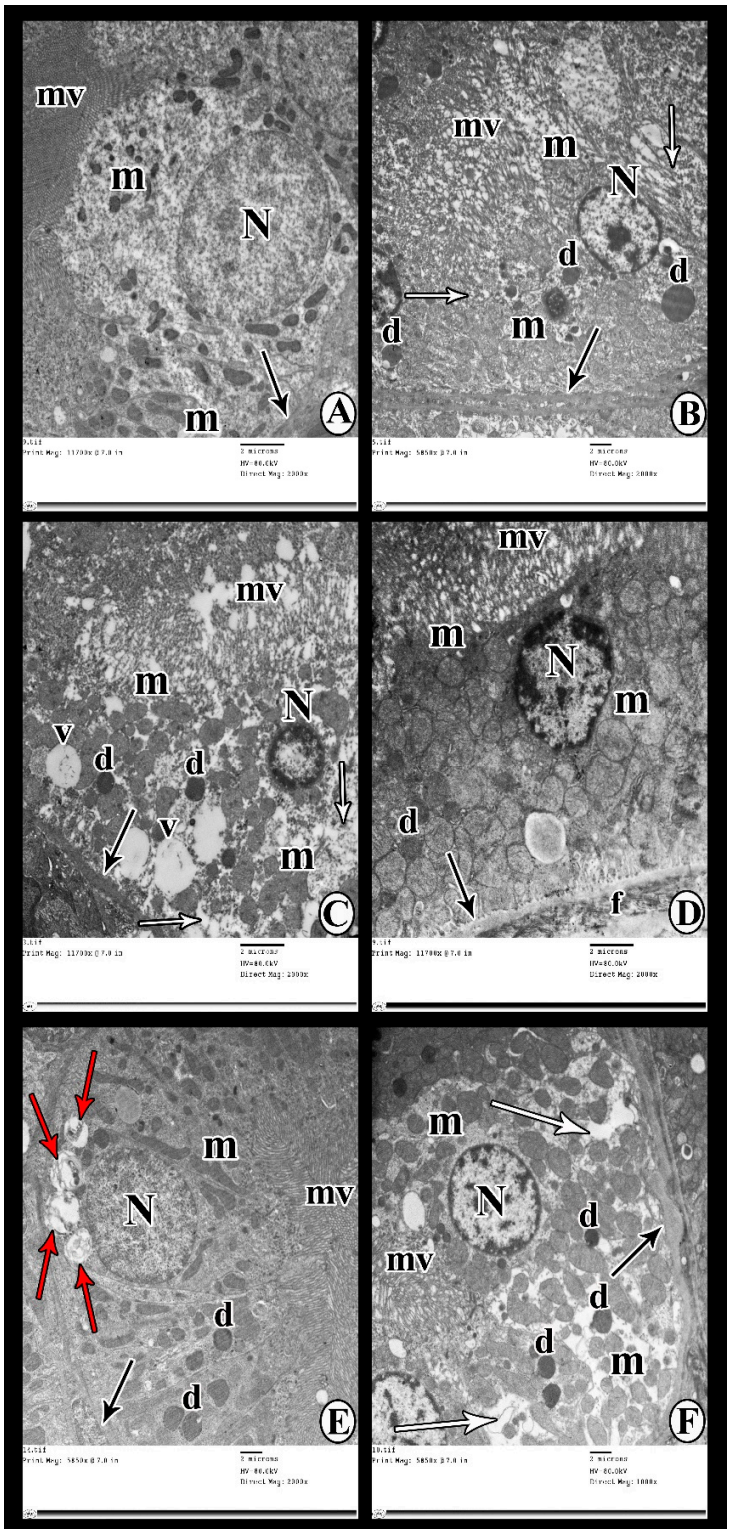

Preprints (www.preprints.org) | NOT PEER-REVIEWED | Posted: 10 September 2018 doi:10.20944/preprints201809.0153.v1

Figure 9

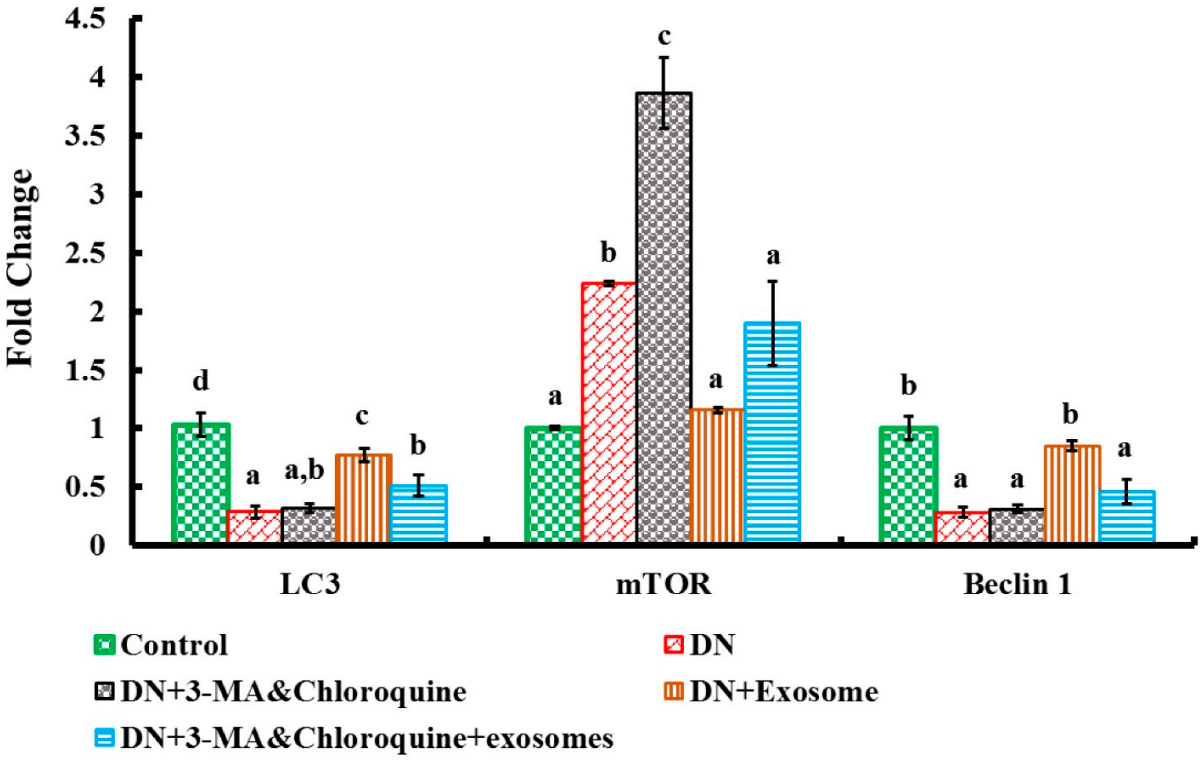

Preprints (www.preprints.org) | NOT PEER-REVIEWED | Posted: 10 September 2018 doi:10.20944/preprints201809.0153.v1

Figure 10